

Alma Mater Studiorum Università di Bologna  
Archivio istituzionale della ricerca

Quantifying atmosphere and ocean origins of North American precipitation variability

This is the final peer-reviewed author's accepted manuscript (postprint) of the following publication:

*Published Version:*

Zhang H., Seager R., He J., Diao H., Pascale S. (2021). Quantifying atmosphere and ocean origins of North American precipitation variability. CLIMATE DYNAMICS, 56(11-12), 4051-4074 [10.1007/s00382-021-05685-0].

*Availability:*

This version is available at: <https://hdl.handle.net/11585/850247> since: 2022-01-31

*Published:*

DOI: <http://doi.org/10.1007/s00382-021-05685-0>

*Terms of use:*

Some rights reserved. The terms and conditions for the reuse of this version of the manuscript are specified in the publishing policy. For all terms of use and more information see the publisher's website.

This item was downloaded from IRIS Università di Bologna (<https://cris.unibo.it/>).  
When citing, please refer to the published version.

(Article begins on next page)

This is the final peer-reviewed accepted manuscript of:

Zhang, H., Seager, R., He, J. et al. *Quantifying atmosphere and ocean origins of North American precipitation variability*. *Climate Dynamics* 56, 4051–4074 (2021).

The final published version is available online at: <https://doi.org/10.1007/s00382-021-05685-0>

#### Rights / License:

The terms and conditions for the reuse of this version of the manuscript are specified in the publishing policy. For all terms of use and more information see the publisher's website.

This item was downloaded from IRIS Università di Bologna (<https://cris.unibo.it/>)

**When citing, please refer to the published version.**

# Quantifying Atmosphere and Ocean origins of North American Precipitation Variability

Honghai Zhang<sup>1\*</sup>, Richard Seager<sup>1</sup>, Jie He<sup>2</sup>, Hansheng Diao<sup>3</sup> and Salvatore Pascale<sup>4</sup>

1. Lamont-Doherty Earth Observatory, Columbia University, Palisades, New York, USA
2. School of Earth and Atmospheric Sciences, Georgia Institute of Technology, Atlanta, Georgia, USA
3. Yau Mathematical Sciences Center, Tsinghua University, Beijing, China
4. Department of Earth System Science, Stanford University, Stanford, California, USA

\* Corresponding author: Honghai Zhang ([clarkzhang2009@gmail.com](mailto:clarkzhang2009@gmail.com); [hhzhang@ldeo.columbia.edu](mailto:hhzhang@ldeo.columbia.edu)), ORCID: 0000-0001-6838-4950

## Abstract

How atmospheric and oceanic processes control North American precipitation variability has been extensively investigated, and yet debates remain. Here we address this question in a 50km-resolution flux-adjusted global climate model. The high spatial resolution and flux adjustment greatly improve the model's ability to realistically simulate North American precipitation, the relevant tropical and midlatitude variability and their teleconnections. Comparing two millennium-long simulations with and without an interactive ocean, we find that the leading modes of North American precipitation variability on seasonal and longer timescales exhibit nearly identical spatial and spectral characteristics, explained fraction of total variance and associated atmospheric circulation. This finding suggests that these leading modes arise from internal atmospheric dynamics and atmosphere-land coupling. However, in the fully coupled simulation, North American precipitation variability still correlates significantly with tropical ocean variability, consistent with observations and prior literature. We find that tropical ocean variability does not create its own type of atmospheric variability but excites internal atmospheric modes of variability in midlatitudes. This oceanic impact on North American precipitation is secondary to atmospheric impacts based on correlation. However, relative to the simulation without an interactive ocean, the fully coupled simulation amplifies precipitation variance over southwest North America (SWNA) during late spring to summer by up to 90%. The amplification is caused by a stronger variability in atmospheric moisture content that is attributed to tropical Pacific sea surface temperature variability. Enhanced atmospheric moisture variations over the tropical Pacific are transported by seasonal mean southwesterly winds into SWNA, resulting in larger precipitation variance.

## 1. Introduction

Precipitation over North America, a region prone to frequent large-scale droughts persisting from a season to multiple decades (e.g., Seager and Ting 2017), has been extensively studied over the past forty years with a goal to assess its predictability and improve predictions. Most of the efforts have been focused on the physical understanding of North American precipitation variability. Processes underlying North American (or any regional) precipitation variability can be categorized into two types, external radiative forcing and internal climate dynamics. In this work we focus on the latter, which consists of processes internal to, and interactions among, atmosphere, land, cryosphere and ocean, on seasonal and longer timescales.

Precipitation is a meteorological phenomenon and the earliest studies are, as expected, atmosphere-oriented. The most prominent large-scale atmosphere circulation variability that have been identified to affect North American precipitation includes the Pacific North America (PNA) pattern (Wallace and Gutzler 1981) and the North Pacific Oscillation (NPO) pattern (Walker 1924). Both patterns represent variations of background mean flow over the North Pacific/America sector. The PNA depicts planetary-scale coherent strengthening or weakening of a trough in the central North Pacific, a ridge over the Rocky Mountains and a trough over southeast North America, while the NPO delineates the meridional movements of the Asian-Pacific jet. The PNA and NPO affect North American precipitation by modulating the Pacific storm track and moisture transport into North America (e.g., Leathers et al. 1991; Linkin and Nigam 2008; Liu et al. 2017; Chen et al. 2018; references therein). Although the PNA and NPO are often portrayed as atmosphere circulation variability, they especially the PNA can also be triggered by ocean variability (e.g., Horel and Wallace 1981) and act as a teleconnection to link remote ocean impacts to North American precipitation variability (Liu et al. 2017).

The tropical ocean's role in North American precipitation variability began to be noticed and understood first by Bjerknes (1966, 1969) and then in the late 1970s and early 1980s, when the now-well-established Rossby wave and teleconnection dynamics were theorized (Hoskins and Karoly 1981) and applied to link the tropical Pacific El Niño-Southern Oscillation (ENSO) to meteorological anomalies over North America (Rasmusson and Wallace 1983). Rossby waves excited by ENSO-induced rainfall anomalies in the tropical Pacific propagate poleward and eastward along a great circle of the Earth and generate alternating cyclonic and anticyclonic circulation anomalies that are quasi-stationary and akin to the PNA pattern, with centers of

74 action over the North Pacific, western Canada and the southeastern United States. These  
75 circulation anomalies affect the strength and position of the subtropical jet stream over the North  
76 Pacific (stronger and further equatorward during warm El Niño events and vice versa during cold  
77 La Niña events), which then change the associated storminess, moisture transport and  
78 precipitation over North America. This dynamical mechanism has been tested in models (e.g.,  
79 Palmer and Mansfield 1984, 1986; Suarez 1985) and invoked to explain the observed  
80 precipitation variations over North America during major ENSO events (e.g., Ropelewski and  
81 Halpert 1986; Trenberth et al. 1988; Palmer and Branković 1989; Trenberth and Branstator 1992;  
82 Trenberth and Guillemot 1996; Hoerling and Kumar 2003; Schubert et al. 2009). It has also been  
83 shown to operate during non-ENSO seasons such as boreal summer, although the associated  
84 atmosphere teleconnection pattern changes with seasonal mean circulation (e.g., Castro et al.  
85 2001; and references therein).

86         The ENSO teleconnection mechanism has been expanded by Seager et al. (2003, 2005).  
87 They use observations and models to show that ENSO drives a prominent zonally and  
88 hemispherically symmetric component of precipitation variability in the midlatitudes. El Niño  
89 events warm the entire tropical troposphere, which strengthens the subtropical jets in both  
90 hemispheres and pulls them equatorward (opposite for La Niña events). These changes in the  
91 subtropical jets influence the transient eddy momentum fluxes and the eddy-driven mean  
92 meridional circulation, resulting in ascent and more precipitation in the midlatitudes especially  
93 over North America (Seager et al. 2005a).

94         On decadal to multidecadal time scales, in the early 2000s, tropical Pacific low-frequency  
95 variability was found to affect North American precipitation (e.g., McCabe et al. 2004; Schubert  
96 et al. 2004a, b; Seager et al. 2005b). Over the past two decades, tremendous progress has been  
97 made, particularly on decadal droughts over North America (see two review papers by Seager  
98 and Hoerling 2014; Seager and Ting 2017; and the references therein). The dynamical  
99 mechanisms on low-frequency timescales are essentially the same as those on seasonal and  
100 interannual timescales as discussed above.

101         In addition to the tropical Pacific, tropical North Atlantic variability also influences North  
102 American precipitation on seasonal to multidecadal timescales (e.g., Enfield et al. 2001; Sutton  
103 and Hodson 2005, 2007; Wang et al. 2008; Kushnir et al. 2010; Ruprich-Robert et al. 2016,  
104 2018; Johnson et al. 2020). The associated mechanisms are insensitive to timescales (as for the

tropical Pacific), but seasonally dependent (Kushnir et al. 2010). In warm seasons, variations in tropical North Atlantic sea surface temperature (SST) change the strength of the North Atlantic subtropical high (warmer SSTs lead to a weaker high), which influences the associated northward moisture transport on its west flank from the Gulf of Mexico and thus precipitation over North America (mainly the United States and northern Mexico). In cold seasons, the above warm-season mechanism still operates; in addition, tropical North Atlantic SST variations also modify the convection over the equatorial Pacific, which then affects North American precipitation in a way similar to the ENSO teleconnection but with a weaker amplitude. Overall, the impacts of tropical North Atlantic on North American precipitation are considerably weaker than those from the tropical Pacific.

Despite the significant progress on the physical understanding of North American precipitation variability, debates still remain. For example, the argument that the 1988 summer North American drought was caused by the La Niña event that year (Trenberth et al. 1988; Palmer and Branković 1989) has been refuted by others arguing a fundamental role for remote diabatic heating over the western North Pacific as well as local land feedbacks and atmosphere dynamics (Lyon and Dole 1995; Liu et al. 1998; Chen and Newman 1998; Bates et al. 2001, Seager and Hoerling 2014). The attribution of the infamous 1930s Dust Bowl to the persistent cold tropical Pacific and warm tropical North Atlantic (Schubert et al. 2004a, b; Seager et al. 2005b; Herweijer et al. 2006) has been augmented by studies arguing for an indispensable role for human-induced land changes and dust aerosol feedbacks in the persistence, intensification and spatial expansion of the drought (Cook et al. 2009, 2011) and a fundamental role for atmosphere random processes in the onset of the drought (Hoerling et al. 2009). At the core of these debates is a lack of agreement on the relative contributions to North American precipitation of the tropical oceans and internal atmosphere dynamics—processes internal or intrinsic to the atmosphere and independent of other components of the earth system.

The role of internal atmosphere dynamics in North American precipitation variability on seasonal and longer time scales has been emphasized by a few studies (e.g., Hoerling and Kumar 1997; Hoerling et al. 2009; Seager and Hoerling 2014; Stevenson et al. 2014; Seager and Ting 2017; Kumar and Chen 2020). On seasonal to interannual time scales, North American precipitation anomalies during El Niño events differ significantly from event to event (Rasmusson and Wallace 1983), and most of these differences have been attributed to internal

atmosphere variability (Hoerling and Kumar 1997). On decadal time scales, Stevenson et al. (2017) explore the causes of North American megadroughts by comparing a fully coupled simulation with an atmosphere-only simulation driven by climatological SSTs from the coupled simulation. They find similar intensity and frequency of megadroughts between the two simulations and suggest that the atmosphere alone (still coupled with the land) is able to generate North American megadroughts. A recent review paper by Seager and Ting (2017) conclude that the ocean's role in North American decadal droughts is influential, but not paramount, with atmosphere internal variability explaining up to three quarters of the low-frequency precipitation variability. In all of these studies except Stevenson et al., the role of internal atmosphere dynamics is not explicitly assessed, but inferred as a residual between the total precipitation variations and the ocean contributions that are explicitly assessed (often by averaging ensembles of atmosphere-only simulations driven by observed monthly SSTs). Even in Stevenson et al., internal atmosphere dynamics are only assessed as a whole in terms of the statistics of North American megadroughts. It remains unclear how exactly internal atmosphere dynamics work together with ocean variability to generate North American precipitation variability, especially on seasonal and longer timescales.

In this work, we aim to fill this gap by (1) investigating the specific role of internal atmosphere dynamics in North American precipitation variability on seasonal and longer time scales and (2) assessing how atmospheric and oceanic processes play out in the context of North American precipitation variability, that is, how different or comparable the atmosphere-induced and ocean-induced precipitation variability are. We will not only demonstrate the fundamental role of internal atmospheric dynamics and coupling with land in shaping the spatial and spectral characteristics of the leading modes of variability in North American precipitation, but also present a new physical mechanism whereby the tropical oceans affect North American precipitation variability.

## **2. Methods**

### **2.1 Model and experiments**

In order to cleanly separate the contributions of atmospheric and oceanic processes, analyzing observations alone is not enough and we have to use climate models. The model in this work is the Forecast-oriented Low Ocean Resolution (FLOR) flux-adjusted model developed at



the Geophysical Fluid Dynamics Laboratory (Vecchi et al. 2014). FLOR has a high horizontal resolution of approximately 50km for the atmosphere (AM2.5) and land (LM3) components and a horizontal resolution of 1° (telescoping to 0.333° near the equator) for the ocean (MOM4) and sea ice (Sea Ice Simulator) components. It has a standard freely coupled version and a flux-adjusted version. The flux-adjustment in FLOR imposes fixed anomalous enthalpy, momentum and fresh water fluxes to the ocean to correct biases in the climatological seasonal cycle of SST, sea surface salinity and wind stress (against 1979-2012 observations). We use the flux-adjusted FLOR because of its much-improved mean climate and variability (see the next section).

Experiments are summarized in Table 1. We first introduce two long control simulations, one conducted with the fully coupled FLOR for 3500 years and the other with the uncoupled AM2.5 for 1000 years (note in AM2.5, the atmosphere is still coupled with the land). For simplicity, these control simulations are referred to as FLOR and AM2.5, respectively. Both simulations are driven by preindustrial level atmospheric composition and radiative forcing. In AM2.5, the boundary forcing is prescribed as the climatological annual cycle of monthly mean SST and sea ice (concentration and thickness) derived from the last 1000 years of FLOR. This 1000-year FLOR simulation is compared with AM2.5. FLOR and AM2.5 share the same radiative forcing and the same climatology at the surface, but differ in that the ocean (including sea ice) is fully active in FLOR but is replaced with an imposed climatological seasonal cycle of SST and sea ice in AM2.5. Precipitation variability in AM2.5 (excluding seasonal cycle) thus arises purely from internal atmosphere processes and coupling with land, while that in FLOR also includes contributions from the ocean (specifically, SST and sea ice variability). He et al. (2018a) showed that the ocean and atmosphere induced precipitation variability is linearly additive and that variability internal to the atmosphere (and land) can be cleanly extracted using atmosphere-only simulations with prescribed climatological SSTs. Analyzing and comparing the millennium-long fully coupled and atmosphere-only simulations allows for a physically clean and statistically robust assessment of the relative contributions of internal atmosphere processes and coupling with land versus the ocean in North American precipitation variability.

The remaining simulations are summarized in Table 1 and will be introduced later. We first examine the performance of the FLOR model in simulating North American precipitation and the associated climate variability in the tropics and midlatitudes, in order to build confidence

in using the model for investigating North American precipitation variability and the underlying atmospheric and oceanic processes.

## 2.2 Model performance

Precipitation biases over North America, especially over the western mountains, are a common problem in the current generation of climate models (Mejia et al. 2018). The FLOR model, however, substantially reduces these biases owing partly to its high resolution and flux adjustment. A recent paper by Johnson et al. (2020) has explained that the flux adjustment in FLOR reduces SST biases in the tropical Pacific and Atlantic, which improves the climatology of North American precipitation through atmosphere teleconnection mechanisms (including the ENSO teleconnection and those proposed by Kushnir et al. (2010)). Here we highlight the precipitation biases that remain in the flux-adjusted FLOR, against two observational products at 0.5° resolution, the Climatic Research Unit timeseries (CRU) datasets version 3.24.01 (Harris et al. 2014) and the Global Precipitation Climatology Centre (GPCC) version 2018 (Schneider et al. 2011). Fig. 1b shows that the flux-adjusted FLOR still has significant biases over most of North America, with too much precipitation over the Pacific Northwest and the monsoon region and too little precipitation over central to southeast North America. These positive biases are simulated throughout the year while the negative biases occur mainly during early summer to fall (Fig. 17 in appendix). Compared to the climatology, precipitation variability is better simulated in FLOR (Fig. 1c and Fig. 18 in appendix, indicated by more stippling). As will be shown later in the Results section, FLOR realistically simulates the leading modes of North American precipitation variability on seasonal and longer (up to the sampling length) time scales.

Tropical climate variability is assessed by comparing FLOR with the Met Office Hadley Centre's sea ice and sea surface temperature dataset (HadISST) version 1.1 (Rayner 2003). FLOR realistically simulates the spatial pattern and amplitude of tropical SST variability, although the ENSO variability is excessively strong in FLOR (Fig. 2a-b). This bias over the Niño3.4 occurs during February to June, while during the rest of the year FLOR simulates a very realistic Niño3.4 variability (Fig. 2c). FLOR also realistically simulates the ENSO spectrum, with a broad interannual peak consistent with observations (Fig. 2d) but seemingly too weak decadal variability.

To evaluate how FLOR simulates the ENSO teleconnection and impacts on North American precipitation, we compute the correlation coefficients between the Niño3.4 index and

SST, land precipitation and 200mb geopotential height (GHT200) during December to February (DJF). Observational fields include SST from HadISST, precipitation from CRU and geopotential height from the NOAA-CIRES-DOE Twentieth Century Reanalysis (20CR) version 2 (Compo et al. 2011) during 1901-2012. Fig. 3 shows that FLOR simulates the observed global ENSO teleconnection very well, indicated by the similar Rossby wave trains emanating from the tropical Pacific. Over the Pacific/North America sector, FLOR realistically simulates the observed PNA-like upper tropospheric circulation (GHT200) associated with ENSO (Fig. 3a vs 3c). In particular, observed correlations between North American precipitation and ENSO are realistically captured in FLOR, with a pattern of positive/negative correlations over southern/northern North America, respectively (Fig. 3b vs 3d). We note that the correlations appear a bit weaker in FLOR than in observations, which can be partly attributed to the uncertainty in the observed teleconnection patterns due to the insufficient sampling lengths (112 years, (Deser et al. 2017)).

To evaluate FLOR's performance in simulating midlatitude variability over the Pacific/North America sector (20°N-80°N, 100°E-50°W), we conduct an empirical orthogonal function (EOF) decomposition of monthly mean sea level pressure (SLP) variability and compare the leading modes between FLOR and the 20CR dataset (Fig. 4, top two rows). Clearly, FLOR faithfully simulates the top three EOF modes in terms of the spatial pattern and the explained variance. Accounting for about 24% of total variance in both FLOR and 20CR, the first EOF mode (EOF1) features three centers of action over the Aleutian Low, the Arctic Ocean and the Gulf Stream, respectively and likely reflects the surface expression of the PNA (which in literature is defined by middle to upper tropospheric geopotential heights). Note that EOF1 is nearly identical to the ENSO teleconnection pattern in SLP (black contours in Fig. 4 upper left two panels), suggesting that EOF1 is related to the ENSO variability. However, this EOF mode does not owe its existence to ENSO, because it also appears as the first EOF mode in AM2.5 without the interactive varying ocean (Fig. 4 bottom left) and explains a similar amount of monthly SLP variance, 22.7% in AM2.5 vs 24.2% in FLOR. This result supports the familiar concept that ENSO affects the extratropics by projecting onto internal modes of atmospheric variability (e.g., Simmons et al. 1983; Palmer and Mansfield 1984; Geisler et al. 1985; Palmer 1993; Lau and Nath 1994; Saravanan 1998; Hoerling and Kumar 2002; Barsugli and Sardeshmukh 2002; Dai et al. 2017; Henderson et al. 2020). A similar story holds true for the

second and third EOF modes, with EOF2 being the North Pacific Oscillation (Walker 1924) and EOF3 being an east-west seesaw pattern over the Aleutian Islands. Both are realistically simulated in FLOR.

In summary, as shown by Johnson et al. (2020), the flux-adjusted high-resolution FLOR model substantially improves the simulation of North American precipitation climatology compared to its standard version and other peer models. Here we demonstrate that FLOR also realistically simulates climate variability both in the tropical oceans and midlatitudes as well as the ENSO teleconnection. Next, we move on to the focus of this work—North American precipitation variability on seasonal and longer time scales, evaluate how it is simulated in FLOR and investigate how it is shaped by atmospheric and oceanic processes.

### 3. Results

#### 3.1 Dominant modes of variability in North American precipitation

To examine North American precipitation variability on seasonal and longer time scales, we focus on the dominant modes of variability in monthly precipitation calculated from an EOF decomposition. Note that the mean annual cycle has been removed from precipitation prior to the EOF decomposition. In observations and FLOR, the top two EOF modes are significantly separated from each other (and also other modes) based on the North test (North et al. 1982) and reflect the strong precipitation over the southeastern United States and the Pacific Northwest, respectively (recall Fig. 1a). In Fig. 5, for the first matching EOFs, both the observed and FLOR modes have the largest loading over the southeastern United States and explain about 9.0% and 7.8% of their total variance over North America, respectively. In Fig. 6, for the second matching EOFs, the observed and FLOR modes are dominated by two largest loadings along the Pacific Northwest and explains about 6.4% of the variance in observations and 8.8% in FLOR. The pattern correlation between observations and FLOR is 0.77 for the EOF modes in Fig. 5 and 0.87 in Fig. 6. Note that the order of the two modes is reversed between observations and FLOR, with the first (second) mode in observations being the second (first) mode in FLOR. The reversed order in FLOR is due to the relatively large biases in regions of strong precipitation, namely, the Pacific Northwest (more precipitation and larger variance, thus EOF 1) and the southeastern United States (less precipitation and weaker variance, thus EOF 2) (recall Fig. 1c). In addition to the spatial pattern, the principal components (PC) associated with these two EOF modes also

share similar behavior between observations and FLOR: their auto-correlation function decreases to almost zero at the 1-month lag (little or no persistence) and their spectrum is basically flat, both of which are characteristic of a white noise process. Overall, FLOR realistically simulates the spatial and spectral characteristics of the observed dominant modes of variability in monthly mean precipitation over North America. The reversed order of the two leading modes in FLOR and observations suggests that the relative contributions of the two leading modes to total precipitation variability are also reversed, which should be kept in mind for the rest of the paper.

AM2.5 without the interactive ocean simulates virtually the same top two EOF modes as the fully coupled FLOR (Fig. 5 and 6). For both EOF modes, the spatial structure is nearly identical between AM2.5 and FLOR with a pattern correlation of 0.99. The percentage of total variance explained by each EOF mode is also very similar, 8.5% (AM2.5) vs 8.8% (FLOR) for EOF 1 and 7.7% (AM2.5) vs 7.8% (FLOR) for EOF 2. The associated PCs exhibit little or no persistence and have a white-noise spectrum. These similarities suggest that the spatial and spectral characteristics of the two dominant modes of variability in monthly precipitation over North America are not sensitive to the ocean in the FLOR model and are determined by internal atmospheric dynamics and coupling with land.

In addition to monthly precipitation, we have conducted the same EOF decomposition on seasonal mean precipitation and low-pass-filtered monthly precipitation with various cutoff periods (1, 3 and 5 years) and also over various sub-regions of North America. These results are not shown but summarized here. Overall, the spatial pattern of leading EOF modes follows the pattern of strong precipitation (as expected, because strong precipitation implies strong variance and the EOF decomposition by design maximizes the variance explained by the leading modes). The main quantitative difference from the results based on monthly precipitation is in the percentage of explained variance, which increases by various extents depending on the season and the sub-region. However, regardless of seasons and sub-regions, the leading EOF modes of FLOR and AM2.5 still share very similar spatial patterns and white-noise behavior. These similarities further suggest that internal atmospheric dynamics and coupling with land dominate the spatial and spectral characteristics of the leading modes of precipitation variability over North America not only on high-frequency time scales (in monthly precipitation) but also on low-frequency (interannual to decadal) time scales. Next, we return to monthly fields and present the physical processes associated with the two leading EOF modes.

To examine the large-scale atmosphere circulation and possible SST anomalies associated with the top two EOF modes, we calculate the correlation coefficients between the associated PCs and SLP, GHT200 and surface temperature. For the EOF mode with a strong loading over the southeastern United States (Fig. 5), the associated large-scale atmosphere circulation is very similar over North America (where the EOF analysis is performed, indicated by the magenta box in each panel) among observations, FLOR and AM2.5. In Fig. 7, the large-scale pattern of SLP correlation (contours in top row) includes two anticyclones centered around east of the Caribbean and off the Canada-Alaska coast and one cyclone in between over the U.S.. The GHT200 correlation (shading in bottom row) exhibits a similar pattern (but slightly tilted westward), suggesting an equivalent barotropic structure for the associated circulation over North America. The implied geostrophic winds and moisture advection are consistent with the EOF precipitation anomalies. In particular, the moist southerlies from the Gulf of Mexico support the strong precipitation over the southeastern United States, while the wet-dry dipole along the Pacific Northwest (weak in observations but strong in the model simulations) agrees with the wet oceanic southerlies and dry inland northerlies that straddle the anticyclone there.

For the correlation with surface temperature, the local patterns over North America are also very similar among observations, FLOR and AM2.5, and largely consistent with the anomalous advection of mean surface temperature (that is, southerlies lead to warming and vice visa). Remotely over the ocean, the pattern of SST correlation is similar between observations and FLOR (AM2.5 has no SST variability by design). In particular, the EOF mode shown in Fig. 5 is accompanied with positive SST (also increased GHT200 aloft) anomalies over the tropical Pacific and Indian Ocean, suggesting a role for the tropical oceans. However, the weak magnitude of the correlation implies that the role of the tropical oceans is very limited for the variability in monthly precipitation over North America. AM2.5 without the interactive ocean simulates the associated surface temperature and atmospheric circulation over North America (and actually has opposite sign GHT200 anomalies in the tropics), suggesting that the physical processes underlying the precipitation EOF mode shown in Fig. 5 can arise solely from internal atmosphere dynamics and coupling with land.

Similar conclusions are found for the EOF mode shown in Fig. 6 reflecting strong precipitation anomalies over the Pacific coast of North America. In Fig. 8, the associated atmosphere circulation over North America features a strong equivalent-barotropic anticyclone

over the Pacific Northwest in observations, FLOR and AM2.5. To the west of the anticyclone, the associated geostrophic southerlies bring warm moist air from the ocean to British Columbia and Alaska. To the south of the anticyclone geostrophic easterlies bring cold dry air from inland to the US west coast. This results in the dipole pattern in both surface temperature (Fig. 8, shading in top row) and precipitation (Fig. 6). Note that the anticyclone is part of an anomalous circulation that reflects changes in the strength of midlatitude stationary eddies (Fig. 8, contours in bottom row). This EOF mode also exhibits some positive but weak correlations with tropical SSTs, mostly in FLOR. We note that the large-scale atmosphere circulation associated with the two leading EOF modes has three centers of actions over the North Pacific/American sector. These centers of action resemble but are shifted relative to those of the PNA (the upper left two panels in Fig. 4). This difference in atmosphere circulation is consistent with the fact that both of the leading EOF modes in precipitation are different from the precipitation pattern associated with the PNA (not shown but is nearly identical to the ENSO teleconnection pattern in Fig. 3).

Overall, despite the reversed order of the two leading EOF modes, FLOR faithfully reproduces the spatial and spectral features of the observed dominant variability in monthly precipitation over North America and the associated large-scale atmosphere circulation and surface temperature. Comparing the fully coupled FLOR and AM2.5 without the interactive ocean, we find that their dominant modes of monthly (and seasonal) precipitation variability over North America have nearly identical spatial structures, explained fraction of total variance, spectral behavior (no persistence and white-noise spectrum) and the associated large-scale atmosphere circulation and local surface temperature anomalies. These similarities suggest that the dominant variability in North American precipitation arises from internal atmosphere dynamics and coupling with land, and does not require SST variability to exist. However, SST variability, particularly in the tropics, still affects North American precipitation, as demonstrated in the literature and indicated here by the positive correlation with tropical SSTs in FLOR and observations. The weak magnitude of correlation suggests that the impacts of the tropical oceans are very limited. The results that the ocean does not change the spatial and spectral characteristics of North American precipitation leading modes of variability suggest that SST variability does not create its own modes of atmosphere variability but rather excites modes of variability that already exist in the atmosphere. This interpretation is also supported by the results in Fig. 4, where the leading mode of midlatitude variability in AM2.5 without the

interactive ocean is nearly identical to the ENSO teleconnection pattern in the fully coupled FLOR and observations. Note that these results are consistent with the familiar concept that SST variability affects the atmosphere by projecting onto internal modes of atmospheric variability. We emphasize here that SST variability does not significantly change the basic characteristics of the large-scale atmospheric variability and its influence only accounts for a small portion of the total North America precipitation variability. Despite its limited impacts, SST variability is still the main source of long-term predictability for North American precipitation variability beyond the time scales of internal atmosphere dynamics.

### 3.2 Precipitation variance over SWNA

To quantify the impacts of the ocean on year-to-year variance of precipitation over North America, we compute the fractional change of monthly precipitation standard deviation at each grid point for each calendar month between FLOR and AM2.5 by

$$\frac{STD_{FLOR} - STD_{AM2.5}}{STD_{FLOR}} \times 100\%,$$

where  $STD_{FLOR}$  and  $STD_{AM2.5}$  are the year-to-year standard deviation of monthly precipitation evaluated at the same grid point for the same calendar month in FLOR and AM2.5, respectively. In Fig. 9, the impacts of the ocean on precipitation variance are not significant (at 1% level) for most of North America throughout the year. The largest significant fractional increase of precipitation variance due to the ocean occurs over southwest North America (SWNA) during May to about September, with magnitudes up to 90% over parts of SWNA especially the North American monsoon region during June and July. In contrast, during winter (November to February) when ENSO variability peaks (recall Fig. 2c), the fractional increase of precipitation variance is relatively weak and only significant over smaller areas of SWNA.

How does the ocean amplify precipitation variance over SWNA during the late spring through summer? To answer this question, we examine the factors that affect precipitation variability, including evaporation and atmospheric moisture convergence. The latter depends on circulation and moisture variability, which we will focus on. Similar to precipitation, we compute the fractional change in year-to-year standard deviation of these two factors between FLOR and AM2.5. The metrics used are monthly 500mb pressure velocity (Omega500) and column-integrated water vapor (CWV) content. Over SWNA, no systematic significant changes are found in the standard deviation of monthly Omega500 between FLOR and AM2.5 throughout the year (Fig. 10), which suggests that the interactive ocean in FLOR does not



significantly affect the variance of atmosphere divergent circulation over SWNA. In contrast, the standard deviation in CWV is significantly enhanced over SWNA during May to about October (Fig. 11), similar to the changes in precipitation standard deviation (Fig. 9). Together these results suggest that the amplified precipitation variance over SWNA in FLOR relative to AM2.5 is caused by the enhanced variability in atmosphere moisture content.

How does the interactive ocean enhance CWV variability over SWNA and why is this enhancement mainly during late spring to summer but not winter? Our interpretation is that the seasonal mean atmosphere circulation is transporting enhanced CWV anomalies from surrounding oceans into SWNA. This is supported in FLOR by the vertically-integrated fluxes of specific humidity standard deviation by mean winds,  $\int \bar{\vec{u}} \cdot STD(q') dp$ , where  $\bar{\vec{u}}$  is climatological monthly winds,  $STD(q')$  is the standard deviation of monthly specific humidity anomalies and the integral is done for the entire atmosphere. This quantity can also be interpreted as the vertically-integrated mean circulation weighted by moisture variability and thus reflects the mean circulation of the lower troposphere where most of the moisture is. During late spring to early fall (around May to October), CWV variability is significantly enhanced by SST variability over the tropical to midlatitude North Pacific, which extends northeastward into the SWNA region following the mean southwesterly winds (see vectors in Fig. 11). In contrast, during winter (around December to March), the enhanced CWV variability over the northeastern Pacific is confined to the subtropics (presumably owing to the colder atmosphere and smaller moisture capacity in winter) and the mean northwesterly winds are from ocean regions where CWV variability appears insensitive to SST variability, both of which are unfavorable to enhance CWV variability over SWNA.

Which parts of the ocean are responsible for the intensification of precipitation variability over SWNA? To answer this question, we conduct additional experiments (Table 1) that are similar to the AM2.5 simulation but with time varying monthly SSTs from FLOR imposed in different oceans during different times (note that these experiments have first been reported in a companion study focusing on synoptic extreme precipitation in June over SWNA (Zhang 2020)). Four experiments are conducted, each 600 years long (corresponding to FLOR 2601-3200). The first one has monthly SSTs prescribed over the entire globe (for all months, hereafter, Globe\_1-12) to test whether this technique (AM2.5 imposed with monthly SSTs) can reproduce the FLOR precipitation variance over SWNA given that interactive ocean-atmosphere coupling may matter

(e.g., Bretherton and Battisti 2000; He et al. 2017, 2018b). The other three have monthly SSTs prescribed between 35°N and 35°S (with a 5° linear buffer zone) in the entire tropics for all months (Tropic\_1-12), the tropical Pacific for October to May (Pacific\_10-5) and the tropical Atlantic for May to October (Atlantic\_5-10), respectively. The reason for prescribing SSTs in Pacific\_10-5 and Atlantic\_5-10 only during the stated months is that SST correlations with the SWNA precipitation are only significant during the stated months over the respective ocean basins (Fig. 19 in appendix). Tropic\_1-12 can test the role of SSTs in the tropics versus extratropics, while Pacific\_10-5 and Atlantic\_5-10 can test the role of SSTs in the tropical Pacific from October to May and in the tropical Atlantic from May to October, respectively. We note that, in Pacific\_10-5 and Atlantic\_5-10, the May and October SSTs are extrapolated into their neighbor months such that September and June in Pacific\_10-5 and April and November in Atlantic\_5-10 also have anomalous SST forcing (by default in all AM2.5 simulations, monthly SST values are placed in the middle of each month before interpolation onto the model time step). These four experiments allow us to identify the oceans responsible for the amplification of precipitation variance over SWNA.

Compared to AM2.5 without the interactive ocean, Globe\_1-12 generally well reproduces the month-to-month variance (i.e., average of the year-to-year variance over twelve calendar months) of both precipitation and CWV over SWNA in FLOR, albeit a bit weaker and confined to lower latitudes (Fig. 12a-d). These similarities also hold true for the year-to-year variance (Fig. 20-21 in appendix), which justifies the experimental technique to pin down the oceans responsible for the enhanced precipitation variance over SWNA in FLOR. Tropic\_1-12 without extratropical SST variability also well reproduces the precipitation and CWV variance over SWNA in FLOR (Fig. 12e-f for month-to-month variance and Fig. 22-23 for year-to-year variance), suggesting that the tropical SST variability is responsible for the enhanced precipitation variance over SWNA in FLOR.

For the total month-to-month variability, Pacific\_10-5 (Fig. 12g-h) is able to enhance the variance in both CWV and precipitation over most of SWNA, while Atlantic\_5-10 (Fig. 12i-j) only enhances the CWV variance locally in the tropical Atlantic but neither the CWV nor the precipitation variance over SWNA (except southern Mexico and northern central America). For the year-to-year variability, Pacific\_10-5 enhances the precipitation (Fig. 13) and CWV (Fig. 14) variance over SWNA mainly during May and June (recall the extrapolation of SST forcing from

May to June), similar to the enhancement in FLOR, Globe\_1-12 and Tropic\_1-12. In contrast, Atlantic\_5-10 does not simulate systematic enhancement of precipitation (Fig. 15) and CWV (Fig. 16) variance over SWNA during May to October when the SST forcing is imposed in the tropical Atlantic. Together, these results suggest that it is the tropical Pacific that accounts for the enhanced precipitation variance over SWNA in FLOR relative to AM2.5.

The lack of impacts from the tropical Atlantic on the SWNA precipitation variance seems inconsistent with previous studies (Kushnir et al. 2010; Johnson et al. 2020). In particular, Johnson et al. (2020) have attributed most of the climatological precipitation biases over southern North America in the standard FLOR model to the strong SST biases in the tropical North Atlantic. This paradox can be explained by the different magnitudes of SST biases and variability in the tropical North Atlantic relative to the tropical Pacific. The SST biases in the standard FLOR model are much larger in the tropical North Atlantic (about 1-3K) than the tropical Pacific (less than 1K, see Fig. 2 in Johnson et al.), while the total month-to-month variability in the flux-adjusted FLOR is much stronger in the tropical Pacific than the tropical Atlantic (Fig. 2b). Therefore, our results from Atlantic\_5-10 should be interpreted as that SST variability in the tropical Atlantic is relatively weak and unable to significantly affect the variance of atmosphere moisture content and thus precipitation over SWNA. The enhancement of the SWNA precipitation variance in FLOR relative to AM2.5 is mainly caused by the tropical Pacific through the new mechanism proposed in this work.

We point out an important distinction between our new mechanism and the classic ENSO teleconnection mechanism. In the ENSO teleconnection mechanism, tropical Pacific SST anomalies drive anomalous atmosphere circulation over SWNA that is capable of inducing anomalous precipitation. Our mechanism does not directly involve changes in atmosphere circulation over SWNA, but only involve enhanced atmosphere moisture content variability, that is, larger atmosphere moisture content anomalies. A new implication from our mechanism is that an interactive ocean is crucial to simulate and predict the amplitude of precipitation variability (i.e., precipitation intensity) over SWNA.

#### **4. Summary and Discussion**

We have quantified the atmospheric and oceanic contributions to North American precipitation variability on seasonal and longer time scales in the FLOR model. FLOR features a

50km resolution in its atmosphere/land components and flux adjustment to correct biases in mean SST; as a result, it greatly reduces the pervasive biases in North American precipitation that have plagued climate models of the same generation. FLOR also realistically simulates tropical and midlatitude climate variability as well as the ENSO teleconnection, all of which are critical for a reliable quantification of the atmospheric and oceanic contributions to North American precipitation variability.

Comparing two millennium-long simulations with and without an active ocean (FLOR and AM2.5), we find that the dominant modes of variability in North American monthly precipitation between the two simulations share a nearly identical spatial structure, explained fraction of total variance and white-noise spectra with no persistence. Furthermore, the associated large-scale atmosphere circulation and surface temperature anomalies over North America are also very similar in terms of both spatial pattern and magnitude. These similarities suggest that the dominant modes of North American precipitation variability do not owe their existence to the ocean, but rather arise from internal atmosphere processes and coupling with land.

In the fully coupled FLOR, however, the dominant modes of North American precipitation variability are still significantly correlated with the tropical oceans, especially the tropical Pacific and Indian Oceans. These correlations are consistent with observations and previous studies that have demonstrated a role for the tropical oceans. How the tropical oceans affect extratropical climate variability has been long debated, with some arguing that tropical variability exerts its own unique impacts by driving atmospheric circulation anomalies that are distinct from internal modes of atmospheric variability (e.g., Straus and Shukla 2000) but others arguing that tropical variability merely excites modes of variability that already exist in the atmosphere (e.g., Simmons et al. 1983; Palmer and Mansfield 1984; Geisler et al. 1985; Palmer 1993; Lau and Nath 1994; Saravanan 1998; Hoerling and Kumar 2002; Barsugli and Sardeshmukh 2002; Dai et al. 2017; Henderson et al. 2020). Here our results on North American precipitation variability support the latter argument. In particular, the ENSO teleconnection pattern over the Pacific/North America sector in FLOR appears in AM2.5 without the interactive ocean as the leading mode of midlatitude variability. This corroborates the idea that tropical climate variability affects the extratropics by exciting modes of variability that already exist in the atmosphere. Taken together, our modeling results suggest that internal atmosphere dynamics

and coupling with land determine the spatial and spectral characteristics of the leading modes of North American precipitation variability and dictate their explained fraction of total variance, while the tropical oceans contribute by exciting the same atmosphere dynamical processes.

Although the tropical oceans do not change the spatial and spectral characteristics of the leading modes of precipitation variability over the entire North America, they significantly enhance the variance of monthly precipitation over SWNA in FLOR relative to AM2.5. This enhancement in FLOR is seasonal and occurs mainly during late spring through summer when the ENSO variability is weakest (Fig. 2) and the correlation between the tropical Pacific SST and SWNA precipitation is weak or not significant (Fig. 19 in appendix). Examining the two factors critical for land precipitation, we find significant enhancement in the variance of atmosphere moisture content but not of divergent circulation over SWNA. The enhanced variability of atmosphere moisture content over SWNA is traced down to the tropical Pacific, where SST variability amplifies atmosphere moisture content variability, which is then transported into the SWNA region during late spring to summer by the seasonal mean southwesterly winds. This interpretation is different from the classic ENSO teleconnection mechanism not only in that it operates mainly during non-ENSO seasons, but more importantly, because it involves a different pathway of influence from the northeastern tropical Pacific to SWNA that is associated with the mean circulation and moisture anomalies as opposed to the dominance of anomalous circulation in the classic ENSO teleconnection mechanism. Therefore, our interpretation is a new mechanism, in addition to the classic ENSO teleconnection, via which the tropical Pacific Ocean variability affects precipitation over SWNA. Note that this mechanism has been invoked in a companion study (Zhang 2020) to explain how the tropical Pacific intensifies extreme rainfall over parts of SWNA in June. Here we extend the mechanism from synoptic time scales to seasonal and longer time scales.

We point out that the amplification of the SWNA precipitation variability by the tropical oceans has been noted by Seager et al. (2014, see their Fig. 5 and the relevant discussions), but their presumed interpretation is the classic ENSO teleconnection. In addition, projected future amplification in hydroclimate variability (Seager et al. 2011; Pendergrass et al. 2017) has been attributed to global warming-induced increases in *mean* atmosphere moisture content via the thermodynamic Clausius-Clapeyron relationship. Our work differs from those projection studies in that we focus on internal climate variability for a constant radiative forcing with a steady

atmosphere moisture content climatology. The variability in atmosphere moisture content (over the ocean) comes mostly from a dynamical redistribution (i.e., convergence or divergence) of atmosphere moisture induced by SST variability.

SST variability in the tropical Atlantic does not significantly contribute to the amplification of precipitation variance over SWNA (except for southern Mexico and northern central America), in contrast to previous studies demonstrating a role for the tropical North Atlantic. This paradox is likely attributed to the weak amplitude of the tropical Atlantic SST variability, which is unable to enhance the variance of atmosphere moisture content over SWNA. We emphasize that the tropical Atlantic SST variability can still affect the precipitation variability over SWNA through other dynamical processes (Kushnir et al. 2010; Johnson et al. 2020).

The contributions of atmospheric and oceanic processes to North American precipitation variability on seasonal and longer time scales in FLOR are summarized as follows. The spatial and spectral characteristics of the dominant modes of variability in North American monthly (and seasonal) precipitation along with their explained fraction of total variance are controlled by internal atmosphere processes and coupling with land. Ocean variability, mainly from the tropical oceans, contributes to North American precipitation variability in two ways. First, on continental scales, it dynamically excites the same internal atmosphere processes as above (to some extent, as beating a drum excites its normal modes), and thus does not change the spatial characteristics of the leading modes. This impact is secondary compared to internal atmosphere processes and unable to significantly modify the leading modes' white-noise spectrum and explained fraction of total variance. Nonetheless, this ocean impact provides potential long-term predictability for North American precipitation beyond the timescales limited by internal atmosphere processes. Second, on regional scales, SST variability in the tropical Pacific amplifies atmosphere moisture content variability, which during late spring to summer is transported by mean southwesterly winds into the SWNA region and enhances the variance of precipitation over SWNA. This enhancement implies that the tropical Pacific is required for a reliable simulation and prediction of the intensity of precipitation over SWNA.

## **Acknowledgement**

This work is supported by NSF awards OCE-16-57209 and AGS-19-34363. Discussions with Tom Delworth are much appreciated. Comments from three anonymous reviewers help clarify some overlooked issues. GPCP Precipitation data and NOAA-CIRES-DOE Twentieth Century reanalysis products are provided by the NOAA/OAR/ESRL PSD, Boulder, Colorado, USA, from their Web site at <https://www.esrl.noaa.gov/psd/>. All modeling data used here will be available upon request.

## References

- Barsugli JJ, Sardeshmukh PD (2002) Global Atmospheric Sensitivity to Tropical SST Anomalies throughout the Indo-Pacific Basin. *J Climate* 15:3427–3442. [https://doi.org/10.1175/1520-0442\(2002\)015<3427:GASTTS>2.0.CO;2](https://doi.org/10.1175/1520-0442(2002)015<3427:GASTTS>2.0.CO;2)
- Bates GT, Hoerling MP, Kumar A (2001) Central U.S. Springtime Precipitation Extremes: Teleconnections and Relationships with Sea Surface Temperature. *J Climate* 14:3751–3766. [https://doi.org/10.1175/1520-0442\(2001\)014<3751:CUSSPE>2.0.CO;2](https://doi.org/10.1175/1520-0442(2001)014<3751:CUSSPE>2.0.CO;2)
- Bjerknes J (1966) A possible response of the atmospheric Hadley circulation to equatorial anomalies of ocean temperature. *Tellus* 18:820–829. <https://doi.org/10.1111/j.2153-3490.1966.tb00303.x>
- Bjerknes J (1969) ATMOSPHERIC TELECONNECTIONS FROM THE EQUATORIAL PACIFIC. *Mon Wea Rev* 97:163–172. [https://doi.org/10.1175/1520-0493\(1969\)097<0163:ATFTEP>2.3.CO;2](https://doi.org/10.1175/1520-0493(1969)097<0163:ATFTEP>2.3.CO;2)
- Bretherton CS, Battisti DS (2000) An interpretation of the results from atmospheric general circulation models forced by the time history of the observed sea surface temperature distribution. *Geophys Res Lett* 27:767–770. <https://doi.org/10.1029/1999GL010910>
- Castro CL, McKee TB, Pielke RA (2001) The Relationship of the North American Monsoon to Tropical and North Pacific Sea Surface Temperatures as Revealed by Observational Analyses. *Journal of Climate* 14:4449–4473. [https://doi.org/10.1175/1520-0442\(2001\)014<4449:TROTNA>2.0.CO;2](https://doi.org/10.1175/1520-0442(2001)014<4449:TROTNA>2.0.CO;2)
- Chen P, Newman M (1998) Rossby Wave Propagation and the Rapid Development of Upper-Level Anomalous Anticyclones during the 1988 U.S. Drought. *J Climate* 11:2491–2504. [https://doi.org/10.1175/1520-0442\(1998\)011<2491:RWPATR>2.0.CO;2](https://doi.org/10.1175/1520-0442(1998)011<2491:RWPATR>2.0.CO;2)
- Chen Z, Gan B, Wu L, Jia F (2018) Pacific-North American teleconnection and North Pacific Oscillation: historical simulation and future projection in CMIP5 models. *Clim Dyn* 50:4379–4403. <https://doi.org/10.1007/s00382-017-3881-9>

632 Compo GP, Whitaker JS, Sardeshmukh PD, et al (2011) The Twentieth Century Reanalysis  
633 Project. Quarterly Journal of the Royal Meteorological Society 137:1–28.  
634 <https://doi.org/10.1002/qj.776>

635 Cook BI, Miller RL, Seager R (2009) Amplification of the North American “Dust Bowl” drought  
636 through human-induced land degradation. PNAS 106:4997–5001.  
637 <https://doi.org/10.1073/pnas.0810200106>

638 Cook BI, Seager R, Miller RL (2011) Atmospheric circulation anomalies during two persistent  
639 north american droughts: 1932–1939 and 1948–1957. Clim Dyn 36:2339–2355.  
640 <https://doi.org/10.1007/s00382-010-0807-1>

641 Dai Y, Feldstein SB, Tan B, Lee S (2017) Formation Mechanisms of the Pacific–North American  
642 Teleconnection with and without Its Canonical Tropical Convection Pattern. J Climate  
643 30:3139–3155. <https://doi.org/10.1175/JCLI-D-16-0411.1>

644 Deser C, Simpson IR, McKinnon KA, Phillips AS (2017) The Northern Hemisphere Extratropical  
645 Atmospheric Circulation Response to ENSO: How Well Do We Know It and How Do We  
646 Evaluate Models Accordingly? J Climate 30:5059–5082. [https://doi.org/10.1175/JCLI-D-](https://doi.org/10.1175/JCLI-D-16-0844.1)  
647 16-0844.1

648 Enfield DB, Mestas-Nuñez AM, Trimble PJ (2001) The Atlantic Multidecadal Oscillation and its  
649 relation to rainfall and river flows in the continental U.S. Geophysical Research Letters  
650 28:2077–2080. <https://doi.org/10.1029/2000GL012745>

651 Geisler JE, Blackmon ML, Bates GT, Muñoz S (1985) Sensitivity of January Climate Response to  
652 the Magnitude and Position of Equatorial Pacific Sea Surface Temperature Anomalies. J  
653 Atmos Sci 42:1037–1049. [https://doi.org/10.1175/1520-](https://doi.org/10.1175/1520-0469(1985)042<1037:SOJCRT>2.0.CO;2)  
654 0469(1985)042<1037:SOJCRT>2.0.CO;2

655 Harris I, Jones P d., Osborn T j., Lister D h. (2014) Updated high-resolution grids of monthly  
656 climatic observations – the CRU TS3.10 Dataset. Int J Climatol 34:623–642.  
657 <https://doi.org/10.1002/joc.3711>

658 He J, Deser C, Soden BJ (2017) Atmospheric and Oceanic Origins of Tropical Precipitation  
659 Variability. J Climate 30:3197–3217. <https://doi.org/10.1175/JCLI-D-16-0714.1>

660 He J, Johnson NC, Vecchi GA, et al (2018a) Precipitation Sensitivity to Local Variations in  
661 Tropical Sea Surface Temperature. Journal of Climate 31:9225–9238.  
662 <https://doi.org/10.1175/JCLI-D-18-0262.1>

663 He J, Kirtman B, Soden BJ, et al (2018b) Impact of Ocean Eddy Resolution on the Sensitivity of  
664 Precipitation to CO2 Increase. Geophysical Research Letters 45:7194–7203.  
665 <https://doi.org/10.1029/2018GL078235>



666 Henderson SA, Vimont DJ, Newman M (2020) The Critical Role of Non-Normality in Partitioning  
667 Tropical and Extratropical Contributions to PNA Growth. *J Climate* 33:6273–6295.  
668 <https://doi.org/10.1175/JCLI-D-19-0555.1>

669 Herweijer C, seager richard, Cook ER (2006) North American droughts of the mid to late  
670 nineteenth century: a history, simulation and implication for Mediaeval drought. *The*  
671 *Holocene*

672 Hoerling M, Kumar A (2003) The Perfect Ocean for Drought. *Science* 299:691–694.  
673 <https://doi.org/10.1126/science.1079053>

674 Hoerling M, Quan X-W, Eischeid J (2009) Distinct causes for two principal U.S. droughts of the  
675 20th century. *Geophysical Research Letters* 36:. <https://doi.org/10.1029/2009GL039860>

676 Hoerling MP, Kumar A (1997) Why do North American climate anomalies differ from one El  
677 Niño event to another? *Geophysical Research Letters* 24:1059–1062.  
678 <https://doi.org/10.1029/97GL00918>

679 Hoerling MP, Kumar A (2002) Atmospheric Response Patterns Associated with Tropical Forcing.  
680 *J Climate* 15:2184–2203. [https://doi.org/10.1175/1520-](https://doi.org/10.1175/1520-0442(2002)015<2184:ARPAWT>2.0.CO;2)  
681 [0442\(2002\)015<2184:ARPAWT>2.0.CO;2](https://doi.org/10.1175/1520-0442(2002)015<2184:ARPAWT>2.0.CO;2)

682 Horel JD, Wallace JM (1981) Planetary-Scale Atmospheric Phenomena Associated with the  
683 Southern Oscillation. *Monthly Weather Review* 109:813–829.  
684 [https://doi.org/10.1175/1520-0493\(1981\)109<0813:PSAPAW>2.0.CO;2](https://doi.org/10.1175/1520-0493(1981)109<0813:PSAPAW>2.0.CO;2)

685 Hoskins BJ, Karoly DJ (1981) The Steady Linear Response of a Spherical Atmosphere to Thermal  
686 and Orographic Forcing. *J Atmos Sci* 38:1179–1196. [https://doi.org/10.1175/1520-](https://doi.org/10.1175/1520-0469(1981)038<1179:TSLROA>2.0.CO;2)  
687 [0469\(1981\)038<1179:TSLROA>2.0.CO;2](https://doi.org/10.1175/1520-0469(1981)038<1179:TSLROA>2.0.CO;2)

688 Johnson NC, Krishnamurthy L, Wittenberg AT, et al (2020) The Impact of Sea Surface  
689 Temperature Biases on North American Precipitation in a High-Resolution Climate  
690 Model. *J Climate* 33:2427–2447. <https://doi.org/10.1175/JCLI-D-19-0417.1>

691 Kumar A, Chen M (2020) Understanding Skill of Seasonal Mean Precipitation Prediction over  
692 California during Boreal Winter and Role of Predictability Limits. *J Climate* 33:6141–  
693 6163. <https://doi.org/10.1175/JCLI-D-19-0275.1>

694 Kushnir Y, Seager R, Ting M, et al (2010) Mechanisms of Tropical Atlantic SST Influence on North  
695 American Precipitation Variability. *J Climate* 23:5610–5628.  
696 <https://doi.org/10.1175/2010JCLI3172.1>

697 Lau N-C, Nath MJ (1994) A Modeling Study of the Relative Roles of Tropical and Extratropical  
698 SST Anomalies in the Variability of the Global Atmosphere-Ocean System. *J Climate*  
699 7:1184–1207. [https://doi.org/10.1175/1520-0442\(1994\)007<1184:AMSOTR>2.0.CO;2](https://doi.org/10.1175/1520-0442(1994)007<1184:AMSOTR>2.0.CO;2)

700 Leathers DJ, Yarnal B, Palecki MA (1991) The Pacific/North American Teleconnection Pattern  
 701 and United States Climate. Part I: Regional Temperature and Precipitation Associations.  
 702 Journal of Climate 4:517–528. [https://doi.org/10.1175/1520-](https://doi.org/10.1175/1520-0442(1991)004<0517:TPATPA>2.0.CO;2)  
 703 0442(1991)004<0517:TPATPA>2.0.CO;2

704 Linkin ME, Nigam S (2008) The North Pacific Oscillation–West Pacific Teleconnection Pattern:  
 705 Mature-Phase Structure and Winter Impacts. Journal of Climate 21:1979–1997.  
 706 <https://doi.org/10.1175/2007JCLI2048.1>

707 Liu AZ, Ting M, Wang H (1998) Maintenance of Circulation Anomalies during the 1988 Drought  
 708 and 1993 Floods over the United States. J Atmos Sci 55:2810–2832.  
 709 [https://doi.org/10.1175/1520-0469\(1998\)055<2810:MOCADT>2.0.CO;2](https://doi.org/10.1175/1520-0469(1998)055<2810:MOCADT>2.0.CO;2)

710 Liu Z, Tang Y, Jian Z, et al (2017) Pacific North American circulation pattern links external forcing  
 711 and North American hydroclimatic change over the past millennium. PNAS 114:3340–  
 712 3345. <https://doi.org/10.1073/pnas.1618201114>

713 Lyon B, Dole RM (1995) A Diagnostic Comparison of the 1980 and 1988 U.S. Summer Heat  
 714 Wave-Droughts. J Climate 8:1658–1675. [https://doi.org/10.1175/1520-](https://doi.org/10.1175/1520-0442(1995)008<1658:ADCOTA>2.0.CO;2)  
 715 0442(1995)008<1658:ADCOTA>2.0.CO;2

716 McCabe GJ, Palecki MA, Betancourt JL (2004) Pacific and Atlantic Ocean influences on  
 717 multidecadal drought frequency in the United States. PNAS 101:4136–4141.  
 718 <https://doi.org/10.1073/pnas.0306738101>

719 Mejia JF, Koračin D, Wilcox EM (2018) Effect of coupled global climate models sea surface  
 720 temperature biases on simulated climate of the western United States. International  
 721 Journal of Climatology 38:5386–5404. <https://doi.org/10.1002/joc.5817>

722 North GR, Bell TL, Cahalan RF, Moeng FJ (1982) Sampling Errors in the Estimation of Empirical  
 723 Orthogonal Functions. Mon Wea Rev 110:699–706. [https://doi.org/10.1175/1520-](https://doi.org/10.1175/1520-0493(1982)110<0699:SEITEO>2.0.CO;2)  
 724 0493(1982)110<0699:SEITEO>2.0.CO;2

725 Palmer TN (1993) Extended-Range Atmospheric Prediction and the Lorenz Model. Bull Amer  
 726 Meteor Soc 74:49–65. [https://doi.org/10.1175/1520-](https://doi.org/10.1175/1520-0477(1993)074<0049:ERAPAT>2.0.CO;2)  
 727 0477(1993)074<0049:ERAPAT>2.0.CO;2

728 Palmer TN, Branković Č (1989) The 1988 US drought linked to anomalous sea surface  
 729 temperature. Nature 338:54–57. <https://doi.org/10.1038/338054a0>

730 Palmer TN, Mansfield DA (1984) Response of two atmospheric general circulation models to  
 731 sea-surface temperature anomalies in the tropical East and West Pacific. Nature  
 732 310:483–485. <https://doi.org/10.1038/310483a0>

733 Palmer TN, Mansfield DA (1986) A study of wintertime circulation anomalies during past El Niño  
 734 events using a high resolution general circulation model. I: Influence of model

735 climatology. Quarterly Journal of the Royal Meteorological Society 112:613–638.  
736 <https://doi.org/10.1002/qj.49711247304>

737 Pendergrass AG, Knutti R, Lehner F, et al (2017) Precipitation variability increases in a warmer  
738 climate. Scientific Reports 7:1–9. <https://doi.org/10.1038/s41598-017-17966-y>

739 Rasmusson EM, Wallace JM (1983) Meteorological Aspects of the El Niño/Southern Oscillation.  
740 Science, New Series 222:1195–1202

741 Rayner NA (2003) Global analyses of sea surface temperature, sea ice, and night marine air  
742 temperature since the late nineteenth century. J Geophys Res 108:4407.  
743 <https://doi.org/10.1029/2002JD002670>

744 Ropelewski CF, Halpert MS (1986) North American Precipitation and Temperature Patterns  
745 Associated with the El Niño/Southern Oscillation (ENSO). Mon Wea Rev 114:2352–2362.  
746 [https://doi.org/10.1175/1520-0493\(1986\)114<2352:NAPATP>2.0.CO;2](https://doi.org/10.1175/1520-0493(1986)114<2352:NAPATP>2.0.CO;2)

747 Ruprich-Robert Y, Delworth T, Msadek R, et al (2018) Impacts of the Atlantic Multidecadal  
748 Variability on North American Summer Climate and Heat Waves. J Climate 31:3679–  
749 3700. <https://doi.org/10.1175/JCLI-D-17-0270.1>

750 Ruprich-Robert Y, Msadek R, Castruccio F, et al (2016) Assessing the Climate Impacts of the  
751 Observed Atlantic Multidecadal Variability Using the GFDL CM2.1 and NCAR CESM1  
752 Global Coupled Models. J Climate 30:2785–2810. <https://doi.org/10.1175/JCLI-D-16-0127.1>

754 Saravanan R (1998) Atmospheric Low-Frequency Variability and Its Relationship to Midlatitude  
755 SST Variability: Studies Using the NCAR Climate System Model. J Climate 11:1386–1404.  
756 [https://doi.org/10.1175/1520-0442\(1998\)011<1386:ALFVAI>2.0.CO;2](https://doi.org/10.1175/1520-0442(1998)011<1386:ALFVAI>2.0.CO;2)

757 Schneider U, Becker A, Finger, Peter, et al (2011) GPCC Full Data Reanalysis Version 6.0 at 0.5°:  
758 Monthly Land-Surface Precipitation from Rain-Gauges built on GTS-based and Historic  
759 Data. [https://doi.org/10.5676/DWD\\_GPCC/FD\\_M\\_V7\\_050](https://doi.org/10.5676/DWD_GPCC/FD_M_V7_050)

760 Schubert S, Gutzler D, Wang H, et al (2009) A U.S. CLIVAR Project to Assess and Compare the  
761 Responses of Global Climate Models to Drought-Related SST Forcing Patterns: Overview  
762 and Results. J Climate 22:5251–5272. <https://doi.org/10.1175/2009JCLI3060.1>

763 Schubert SD, Suarez MJ, Pegion PJ, et al (2004a) Causes of Long-Term Drought in the U.S. Great  
764 Plains. J Climate 17:485–503. [https://doi.org/10.1175/1520-0442\(2004\)017<0485:COLDIT>2.0.CO;2](https://doi.org/10.1175/1520-0442(2004)017<0485:COLDIT>2.0.CO;2)

766 Schubert SD, Suarez MJ, Pegion PJ, et al (2004b) On the Cause of the 1930s Dust Bowl. Science  
767 303:1855–1859. <https://doi.org/10.1126/science.1095048>

768 Seager R, Harnik N, Kushnir Y, et al (2003) Mechanisms of Hemispherically Symmetric Climate  
 769 Variability. *J Climate* 16:2960–2978. [https://doi.org/10.1175/1520-](https://doi.org/10.1175/1520-0442(2003)016<2960:MOHSCV>2.0.CO;2)  
 770 0442(2003)016<2960:MOHSCV>2.0.CO;2

771 Seager R, Harnik N, Robinson WA, et al (2005a) Mechanisms of ENSO-forcing of hemispherically  
 772 symmetric precipitation variability. *Quarterly Journal of the Royal Meteorological*  
 773 *Society* 131:1501–1527. <https://doi.org/10.1256/qj.04.96>

774 Seager R, Hoerling M (2014) Atmosphere and Ocean Origins of North American Droughts. *J*  
 775 *Climate* 27:4581–4606. <https://doi.org/10.1175/JCLI-D-13-00329.1>

776 Seager R, Kushnir Y, Herweijer C, et al (2005b) Modeling of Tropical Forcing of Persistent  
 777 Droughts and Pluvials over Western North America: 1856–2000. *J Climate* 18:4065–  
 778 4088. <https://doi.org/10.1175/JCLI3522.1>

779 Seager R, Naik N, Vogel L (2011) Does Global Warming Cause Intensified Interannual  
 780 Hydroclimate Variability? *J Climate* 25:3355–3372. [https://doi.org/10.1175/JCLI-D-11-](https://doi.org/10.1175/JCLI-D-11-00363.1)  
 781 00363.1

782 Seager R, Ting M (2017) Decadal Drought Variability Over North America: Mechanisms and  
 783 Predictability. *Curr Clim Change Rep* 1–9. <https://doi.org/10.1007/s40641-017-0062-1>

784 Simmons AJ, Wallace JM, Branstator GW (1983) Barotropic Wave Propagation and Instability,  
 785 and Atmospheric Teleconnection Patterns. *J Atmos Sci* 40:1363–1392.  
 786 [https://doi.org/10.1175/1520-0469\(1983\)040<1363:BWPAIA>2.0.CO;2](https://doi.org/10.1175/1520-0469(1983)040<1363:BWPAIA>2.0.CO;2)

787 Stevenson S, Timmermann A, Chikamoto Y, et al (2014) Stochastically Generated North  
 788 American Megadroughts. *J Climate* 28:1865–1880. [https://doi.org/10.1175/JCLI-D-13-](https://doi.org/10.1175/JCLI-D-13-00689.1)  
 789 00689.1

790 Straus DM, Shukla J (2000) Distinguishing between the SST-forced variability and internal  
 791 variability in mid latitudes: Analysis of observations and GCM simulations. *Quarterly*  
 792 *Journal of the Royal Meteorological Society* 126:2323–2350.  
 793 <https://doi.org/10.1002/qj.49712656716>

794 Suarez MJ (1985) Chapter 43 A GCM study of the atmospheric response to tropical SST  
 795 Anomalies. In: Nihoul JCJ (ed) Elsevier Oceanography Series. Elsevier, pp 749–764

796 Sutton RT, Hodson DLR (2005) Atlantic Ocean Forcing of North American and European Summer  
 797 Climate. *Science* 309:115–118. <https://doi.org/10.1126/science.1109496>

798 Sutton RT, Hodson DLR (2007) Climate Response to Basin-Scale Warming and Cooling of the  
 799 North Atlantic Ocean. *J Climate* 20:891–907. <https://doi.org/10.1175/JCLI4038.1>

800 Trenberth KE, Branstator GW (1992) Issues in Establishing Causes of the 1988 Drought over  
801 North America. *J Climate* 5:159–172. [https://doi.org/10.1175/1520-](https://doi.org/10.1175/1520-0442(1992)005<0159:IIECOT>2.0.CO;2)  
802 0442(1992)005<0159:IIECOT>2.0.CO;2

803 Trenberth KE, Branstator GW, Arkin PA (1988) Origins of the 1988 North American Drought.  
804 *Science* 242:1640–1645. <https://doi.org/10.1126/science.242.4886.1640>

805 Trenberth KE, Guillemot CJ (1996) Physical Processes Involved in the 1988 Drought and 1993  
806 Floods in North America. *J Climate* 9:1288–1298. [https://doi.org/10.1175/1520-](https://doi.org/10.1175/1520-0442(1996)009<1288:PPIITD>2.0.CO;2)  
807 0442(1996)009<1288:PPIITD>2.0.CO;2

808 Vecchi GA, T. DELWORTH, R. GUDGEL, et al (2014) On the Seasonal Forecasting of Regional  
809 Tropical Cyclone Activity. *J Climate* 27:7994–8016. [https://doi.org/10.1175/JCLI-D-14-](https://doi.org/10.1175/JCLI-D-14-00158.1)  
810 00158.1

811 Walker GT (1924) Correlation in Seasonal Variations of Weather, IX. A Further Study of World  
812 Weather. *Mem Indian Meteor Dep* 24:275–332

813 Wallace J, Gutzler D (1981) Teleconnections in the geopotential height field during the Northern  
814 Hemisphere winter. *Mon Weather Rev* 109:784–812

815 Wang C, Lee S-K, Enfield DB (2008) Climate Response to Anomalously Large and Small Atlantic  
816 Warm Pools during the Summer. *J Climate* 21:2437–2450.  
817 <https://doi.org/10.1175/2007JCLI2029.1>

818 Zhang H (2020) Tropical Pacific intensifies June extreme rainfall over Southwestern United  
819 States/Northwestern Mexico. *Clim Dyn*. <https://doi.org/10.1007/s00382-020-05291-6>

820

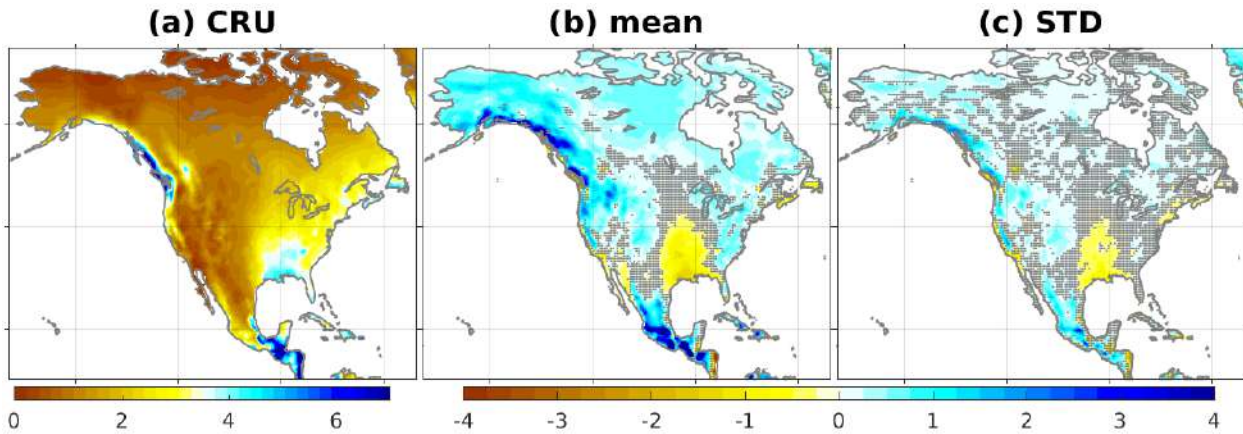
821

Table 1. Simulations.

Experiments	Forcing	Length (yr)
FLOR	preindustrial-level atmospheric composition and radiation (the same for all experiments), flux adjustment	3500
AM2.5	driven by climatological annual cycle of SST and sea ice from last 1000 years of FLOR	1000
Globe_1-12	as AM2.5, but driven by monthly varying SSTs from 600 years of FLOR over entire globe and for all months	600
Tropic_1-12	as AM2.5, but driven by monthly varying SSTs from 600 years of FLOR over the tropics (35°N and 35°S) and for all months	600
Pacific_10-5	as AM2.5, but driven by monthly varying SSTs from 600 years of FLOR over the tropical Pacific (35°N and 35°S) and only from October to May	600
Atlantic_5-10	as AM2.5, but driven by monthly varying SSTs from 600 years of FLOR over the tropical Atlantic (35°N and 35°S) and only from May to October	600

Note that preindustrial radiative forcing is nearly in balance at top of the atmosphere and thus more suitable for millennium-long steady state simulations than present-day conditions.

## Figures



**Fig. 1** Precipitation (mm/day) biases in FLOR compared to observations. (a) 1981-2010 CRU climatology; FLOR biases (FLOR – CRU) in (b) climatology and (c) standard deviation. Stippling is a measure of insignificance, indicating at least one of CRU and GPCC is inside the range of a synthetic 33-member FLOR ensemble, which is constructed by sampling the 1000-year FLOR simulation with a 30-year (to mimic 1981-2010) non-overlapping period.



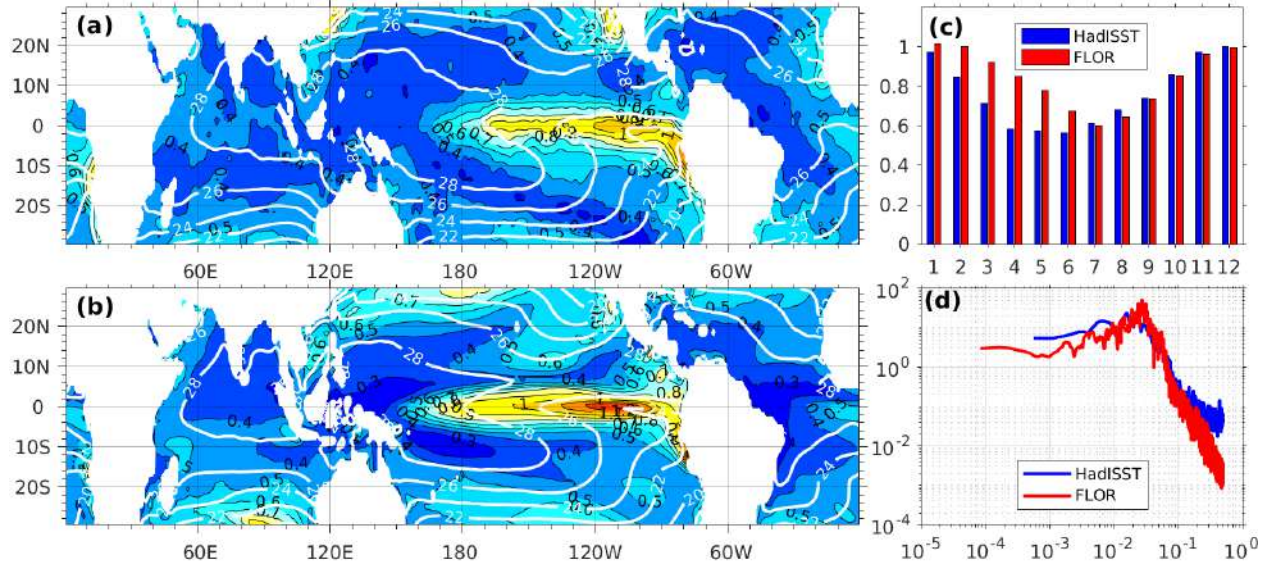


**Fig. 2** Tropical SST variability ( $^{\circ}\text{C}$ ) in FLOR versus HadISST 1870-2018. SST standard deviation (shading) and climatology (white contours) in HadISST (a) and FLOR (b); monthly standard deviation (c) and spectrum (d) of the Niño3.4 index (SST time series averaged over  $170^{\circ}\text{W}$ - $120^{\circ}\text{W}$ ,  $5^{\circ}\text{N}$ - $5^{\circ}\text{S}$ ). The spectrum is normalized by the variance of the Niño3.4 index. X-axis has a unit of calendar month in (c) and frequency of per month in (d), respectively.

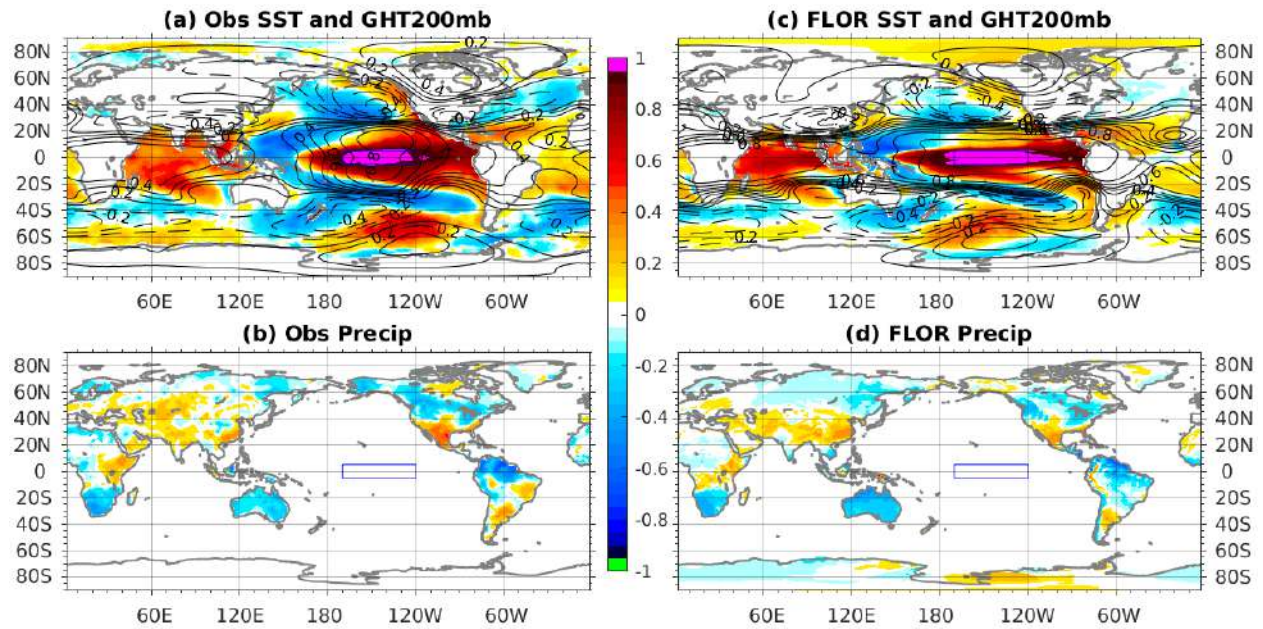


**Fig. 3** ENSO teleconnection in observations 1901-2012 (a, b) and FLOR (c, d). Teleconnection is assessed during DJF as correlation coefficients between the Niño3.4 index and SST (shading), 200mb geopotential height (black contours) in (a, c), land precipitation in (b, d). Here 112 years are used for observations, while 1000 years are used for FLOR. Random sampling of 112-year segments from FLOR leads to small changes in correlation pattern and magnitude (not shown).

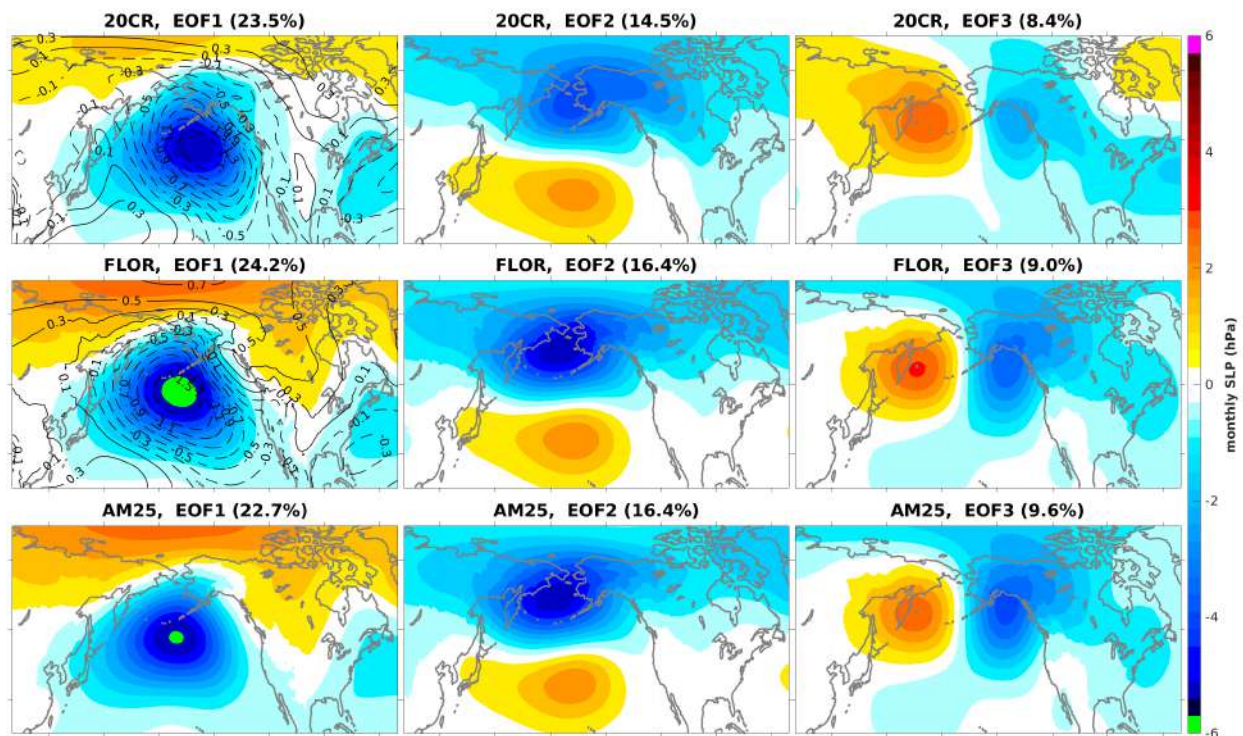


**Fig. 4** Midlatitude variability of monthly SLP (hPa) in observations (top row), FLOR (middle row) and AM2.5 (bottom row). The leading three EOF modes are shown with their explained variance inside the parentheses above each panel. Contours (positive solid and negative dashed) in the EOF1 panels (left column, top two rows) are the regression coefficients (hPa/K) of monthly SLP anomaly against the Niño3.4 index, a measure of the ENSO teleconnection.

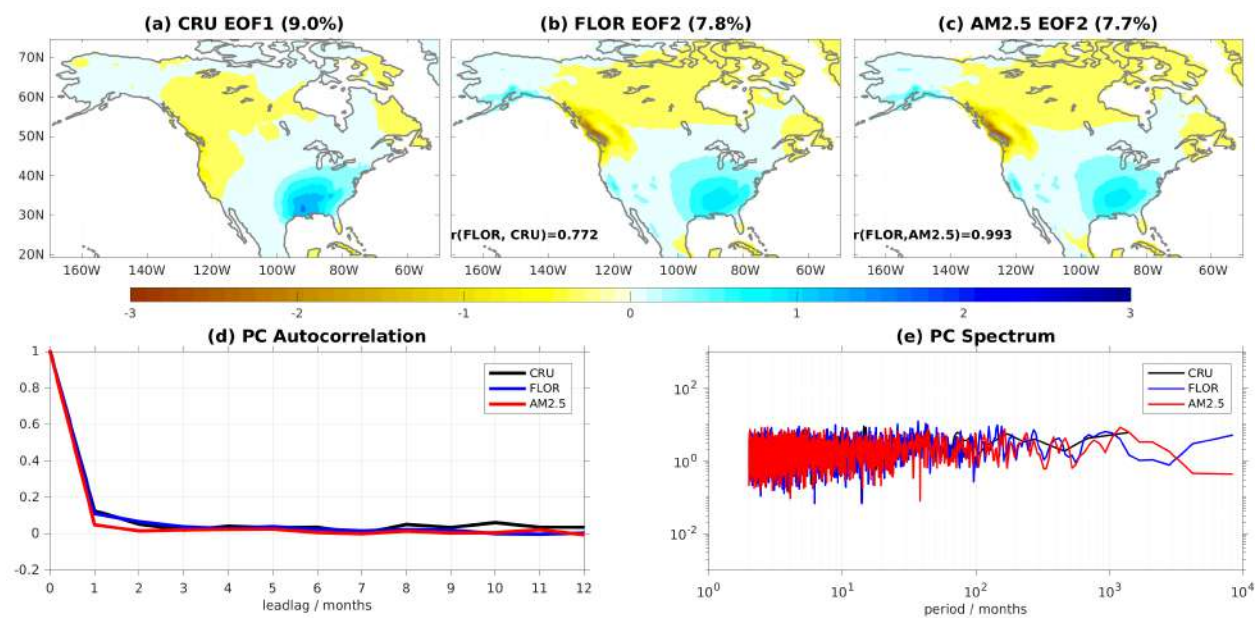




**Fig. 5** Top row: (a) the first EOF mode in CRU observations and the second EOF mode in (b) FLOR and (c) AM2.5. The explained variance percentage is denoted above each panel. Pattern correlation is 0.772 between CRU and FLOR and 0.993 between FLOR and AM2.5. Bottom row: (d) the associated PC autocorrelation and (e) spectrum.

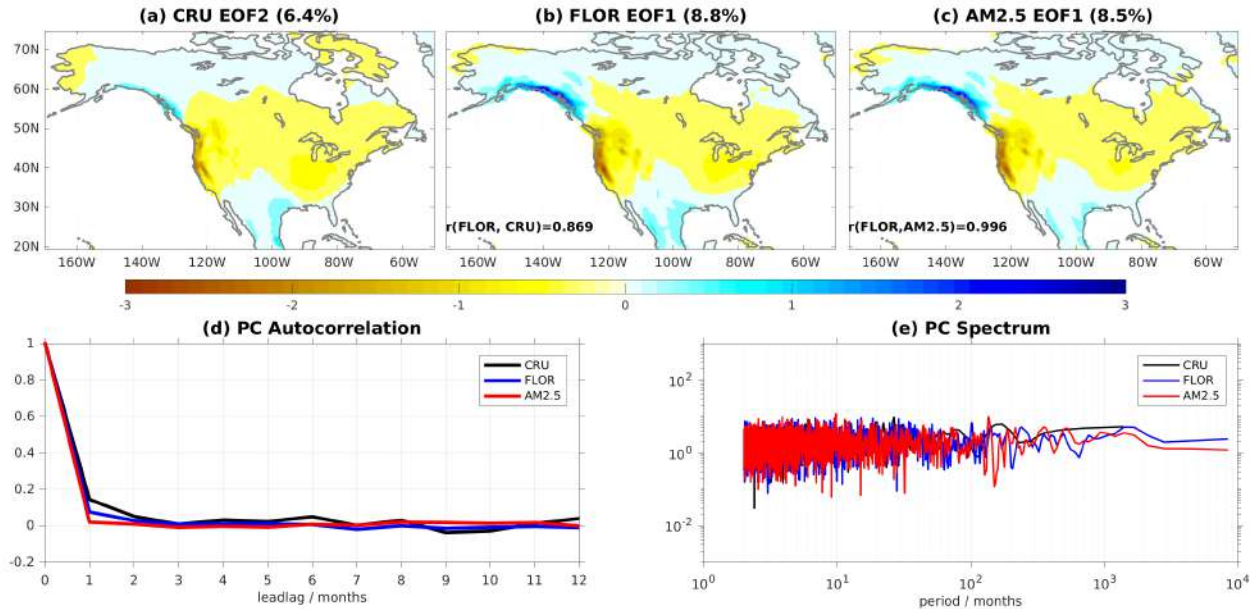


**Fig. 6** The same as Fig. 5 but for the second EOF mode in observations and the first EOF mode in FLOR and AM2.5. Pattern correlation is 0.869 between CRU and FLOR and 0.996 between FLOR and AM2.5.

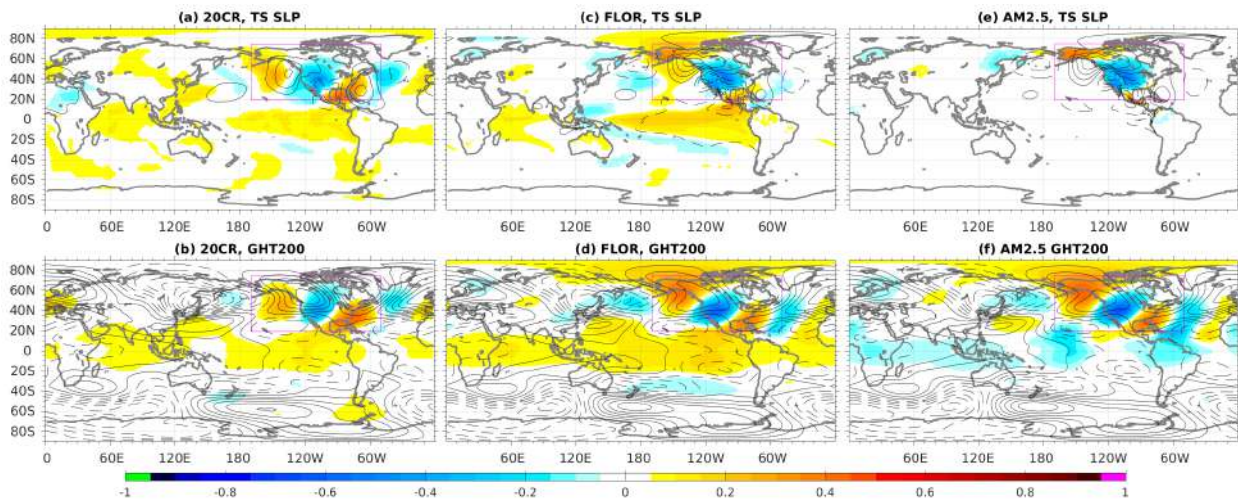


**Fig. 7** Large-scale pattern of correlation coefficients between the PCs of the EOF modes in Fig. 5 (reflecting precipitation variability over the southeastern United States) and surface temperature (shading in top row), SLP (contours in top row) and 200mb geopotential height (shading in bottom row) in observations (left column, 20CR dataset), FLOR (middle column) and AM2.5 (right column). Contours in the bottom row are the departure of climatological GHT200 from its zonal mean, denoting climatological stationary eddies. Contour interval is 0.1 for SLP

correlation and 20m for GHT200, and solid (dashed) contours denote positive (negative) values (zeros omitted). The magenta box in each panel denotes the region where the EOF decomposition is conducted.

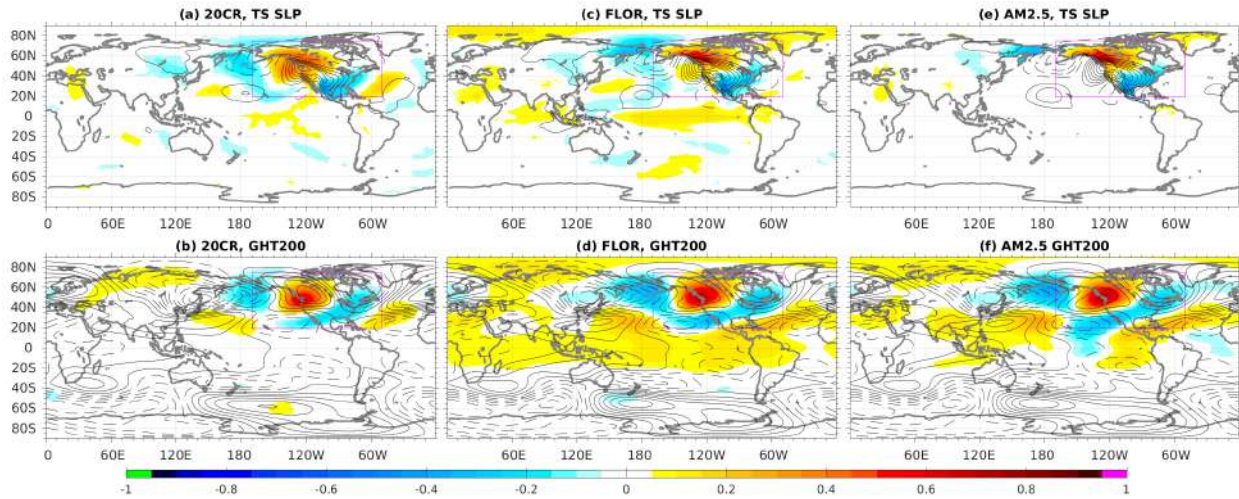


**Fig. 8** The same as Fig. 7 but for the EOF modes shown in Fig. 6 (reflecting precipitation variability over the Pacific Northwest).

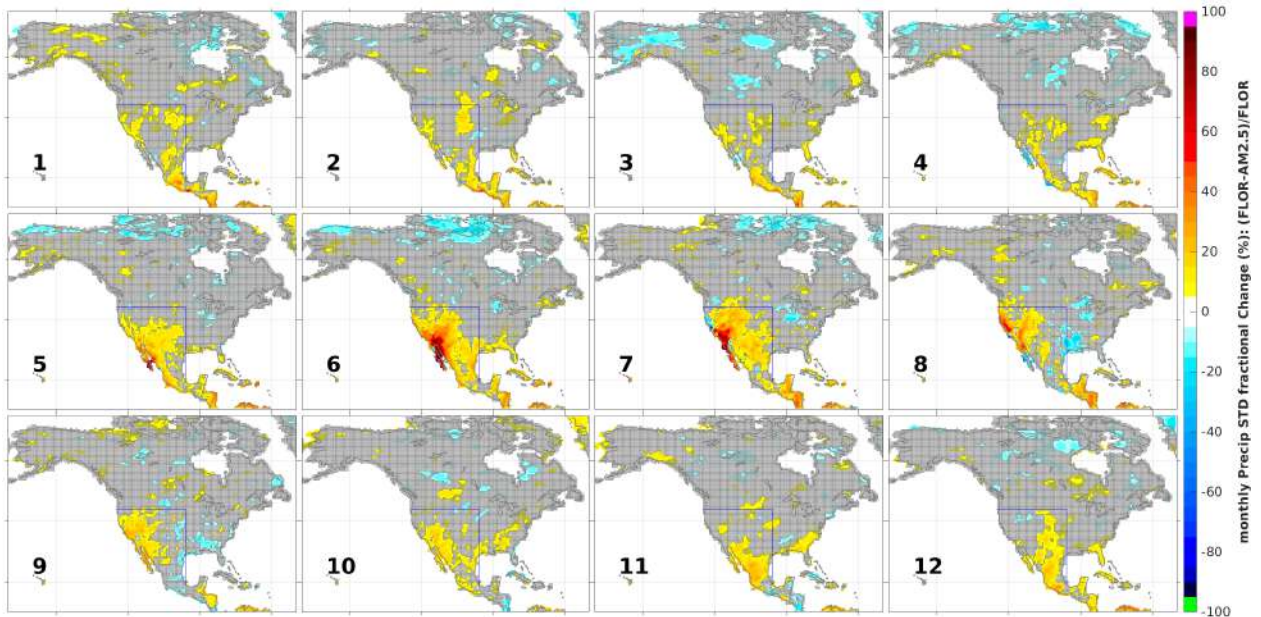


**Fig. 9** Fractional change (%) in year-to-year standard deviation of monthly precipitation between FLOR and AM2.5 as a function of calendar month, defined as  $(\text{FLOR}-\text{AM2.5})/\text{FLOR} \times 100\%$ . Gray stippling indicates changes are not significant at the 1% level based on a two-sided Fisher test. The blue transposed 'L' outlines the SWNA region where the month-to-month variance of monthly precipitation (Fig. 12a) is significantly enhanced by the ocean in FLOR relative to AM2.5.



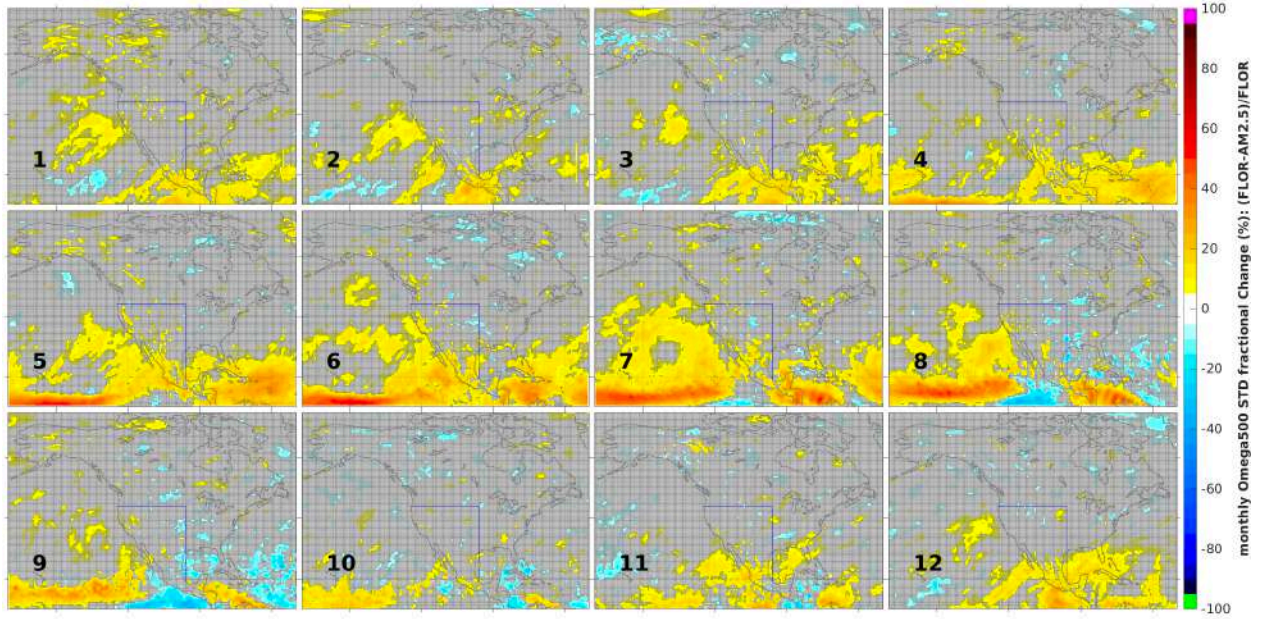


**Fig. 10** The same as Fig. 9 but for 500mb omega.

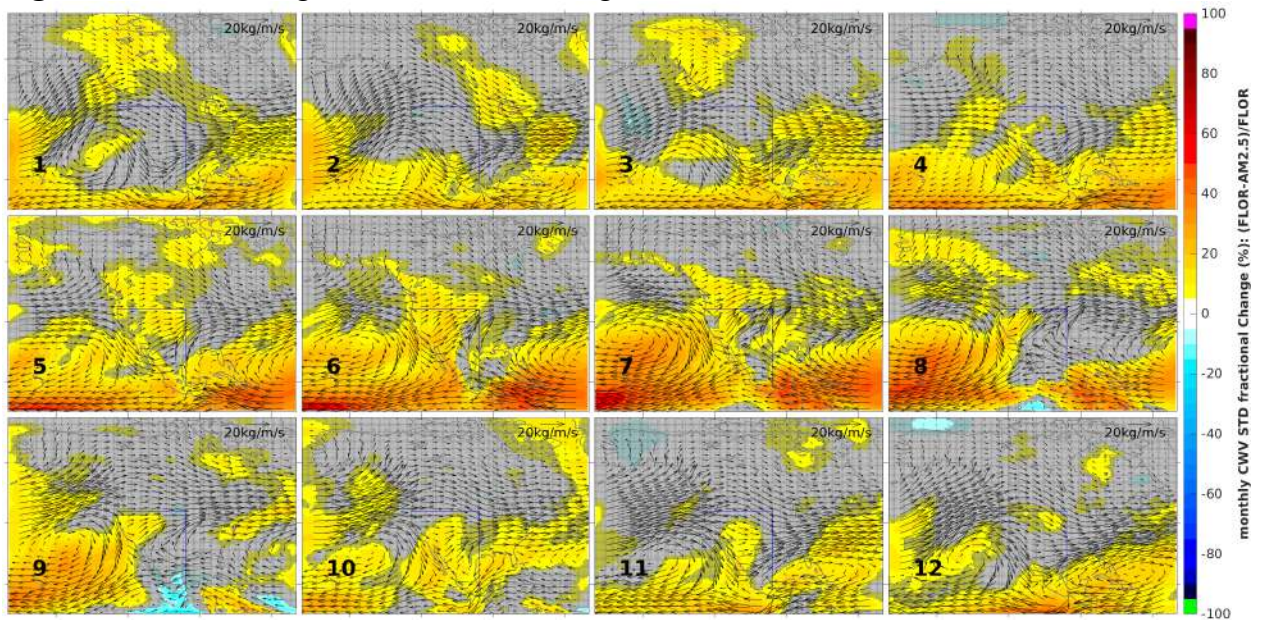


**Fig. 11** The same as Fig. 9 but for CWV (atmosphere moisture content). Vectors denote the vertically integrated flux of standard deviation of specific humidity by mean circulation (kg/m/s). A scale vector of 20kg/m/s is shown in the upper right corner of each panel.



899

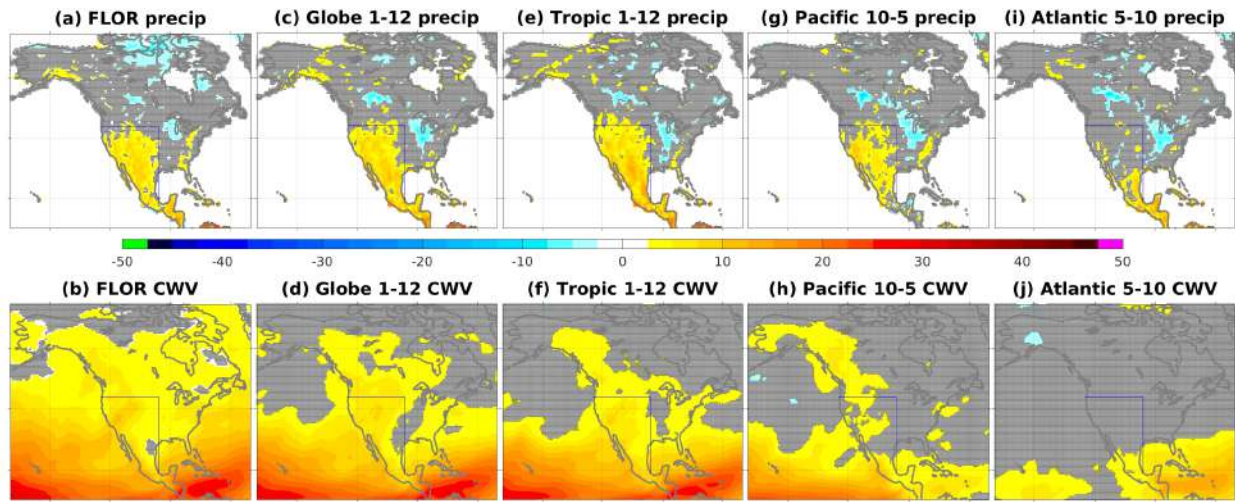


**Fig. 12** Fractional change (%) in monthly precipitation (top row) and CWV (bottom row) month-to-month standard deviation in FLOR (a-b), Globe\_1-12 (c-d), Tropic\_1-12 (e-f), Pacific\_10-5 (g-h) and Atlantic\_5-10 (i-j) with respect to AM2.5. Gray stippling indicates changes are not significant at the 1% level based on a two-sided Fisher test. The blue 'L' outlines the SWNA region.

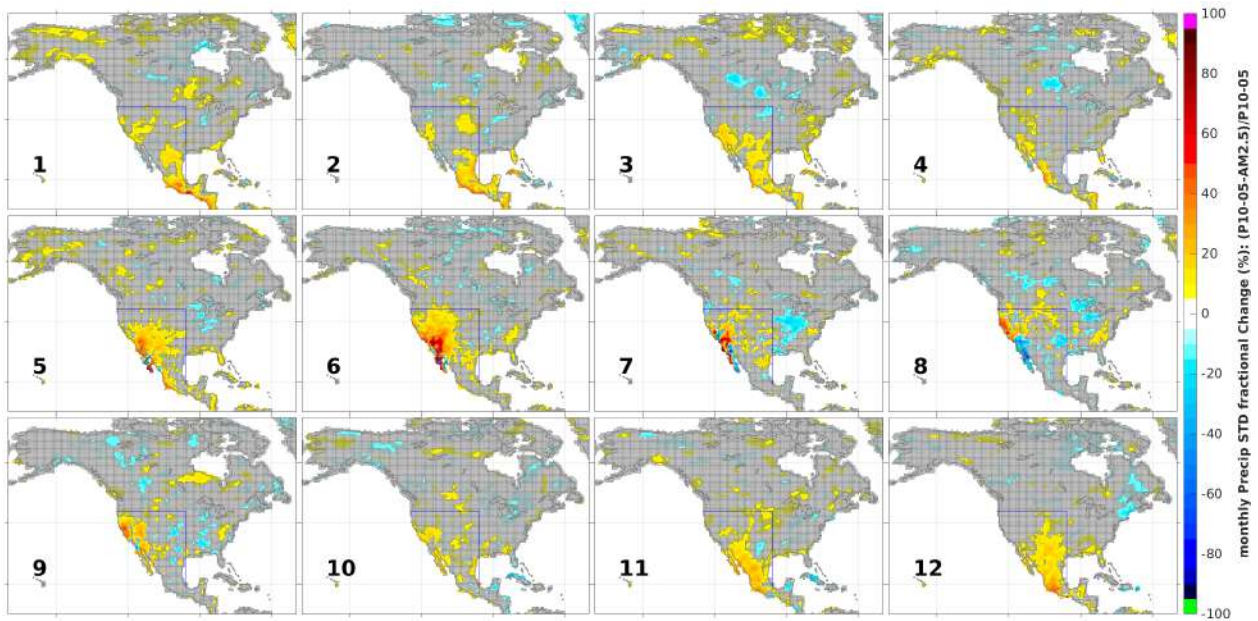
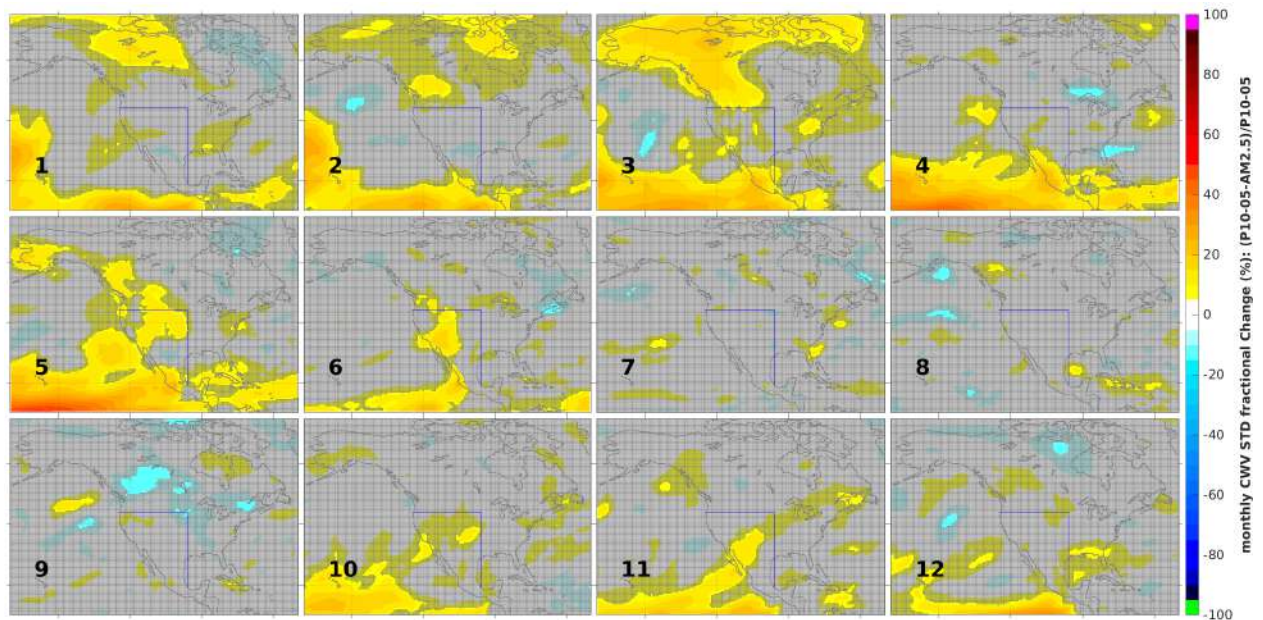


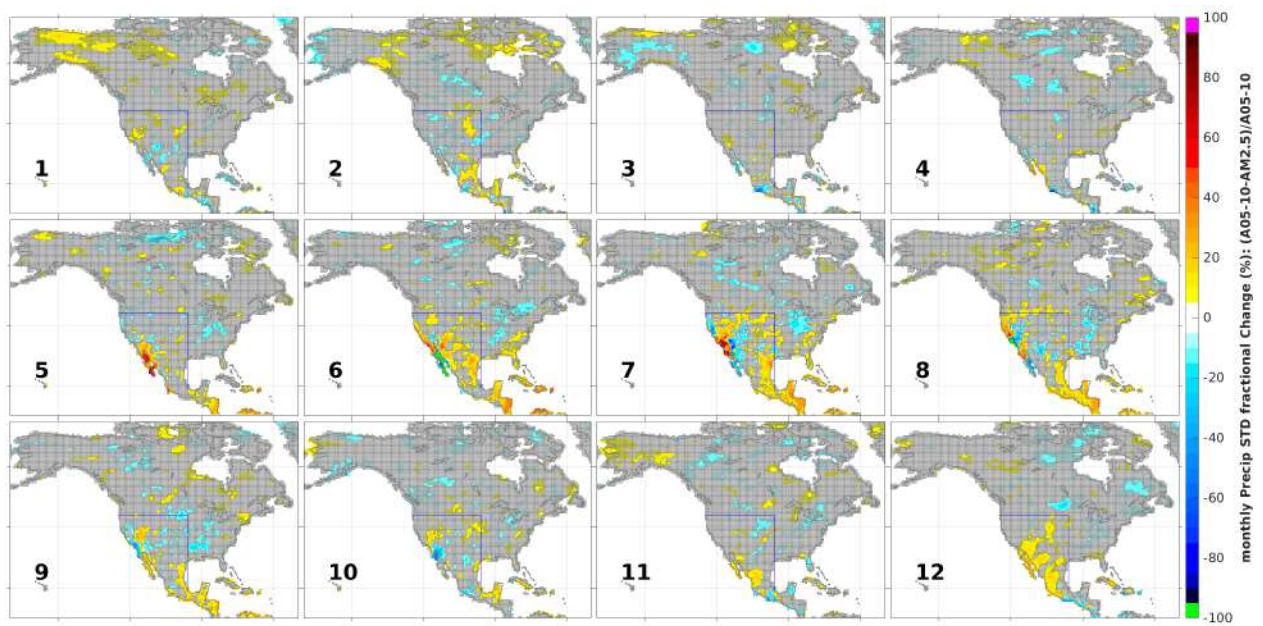
**Fig. 13** The same as Fig. 9 but for Pacific\_10-5.

911



912  
913  
914

**Fig. 14** The same as Fig. 13 but for CWV in Pacific\_10-5.



915  
916

**Fig. 15** The same as Fig. 13 but for Atlantic\_5-10.



917

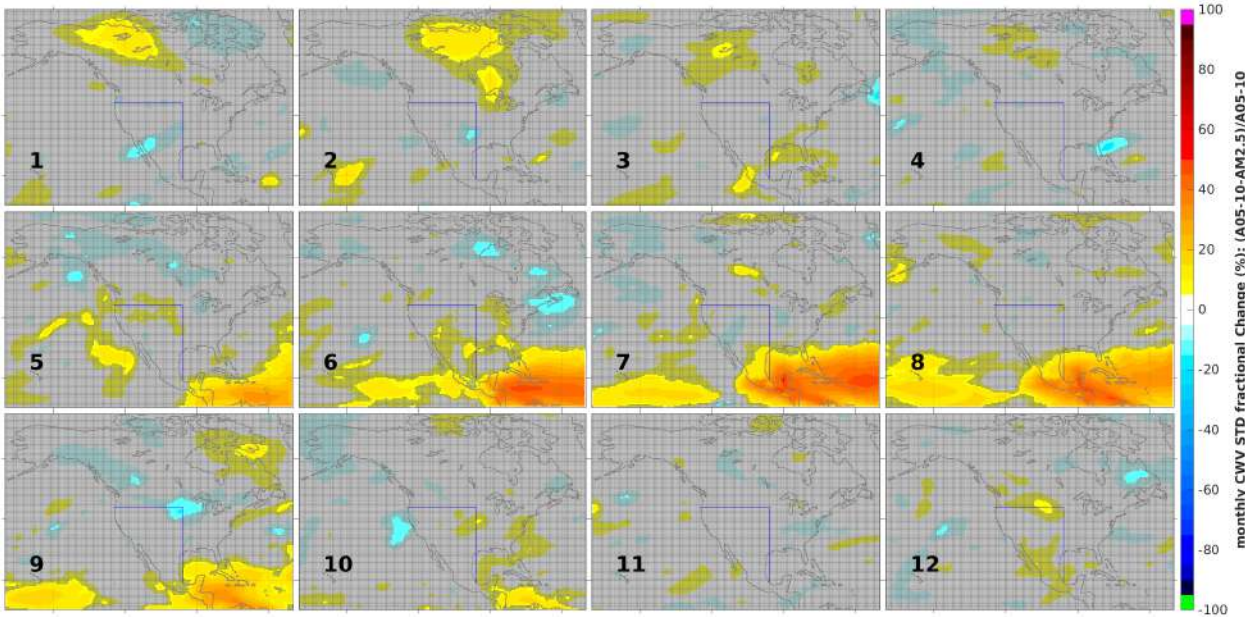


**Fig. 16** The same as Fig. 15 but for CWV in Atlantic\_5-10.

918  
919  
920  
921  
922

## Appendix

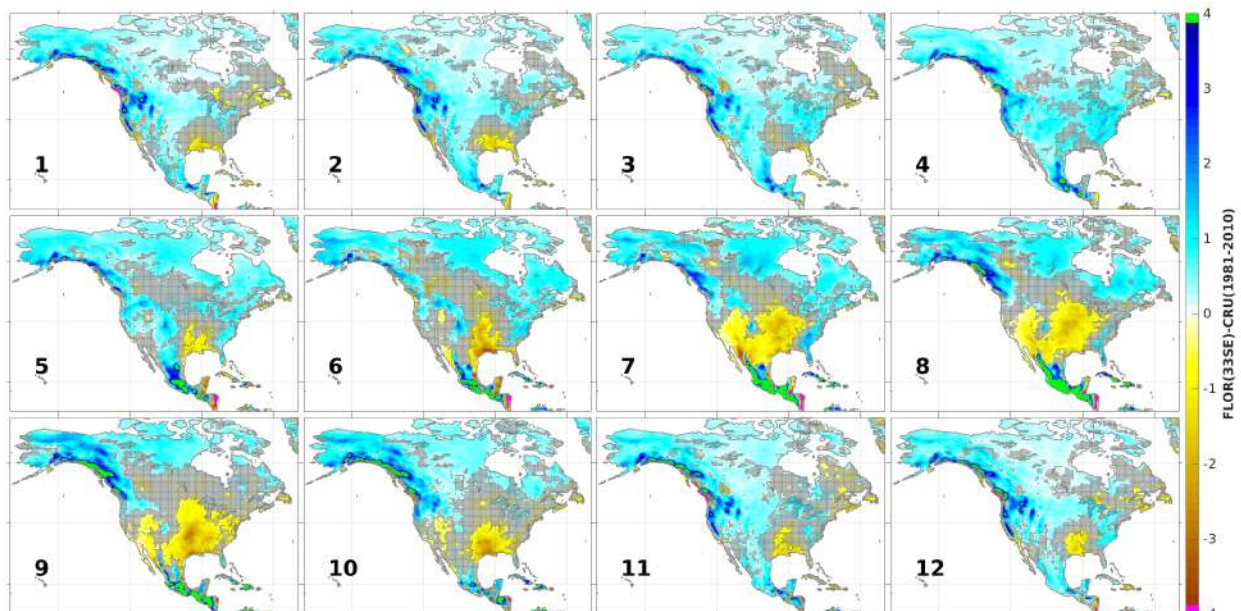


**Fig. 17** Biases of monthly precipitation climatology (mm/day) in FLOR compared to the 1980-2010 CRU and GPCC observations. Shown here is FLOR – CRU. Stippling is measure of insignificance, indicating either CRU or GPCC climatology is inside the range of a synthetic 33-member FLOR ensemble, which is constructed by sampling the 1000-year FLOR simulation with a 30-year non-overlapping period.

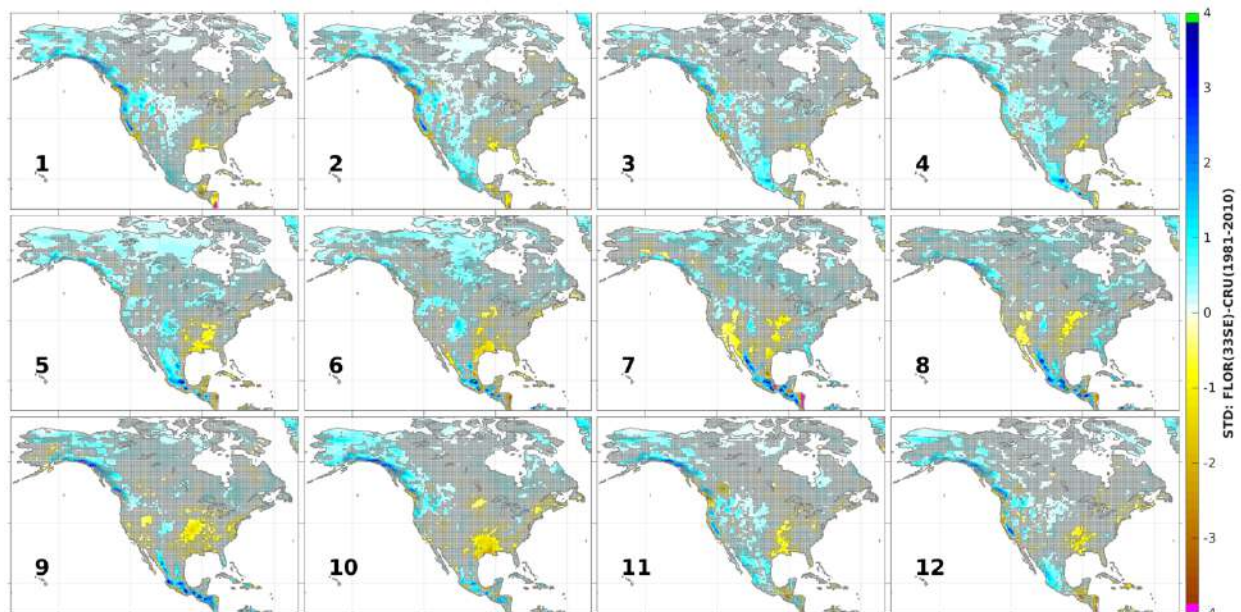


**Fig. 18** Biases in year-to-year standard deviation of monthly precipitation (mm/day) over North America in FLOR compared to the 1980-2010 CRU and GPCC observations. Stippling is a measure of insignificance, indicating either CRU or GPCC standard deviation is inside the range



of a synthetic 33-member FLOR ensemble, which is constructed by sampling the 1000-year FLOR simulation with a 30-year non-overlapping period.

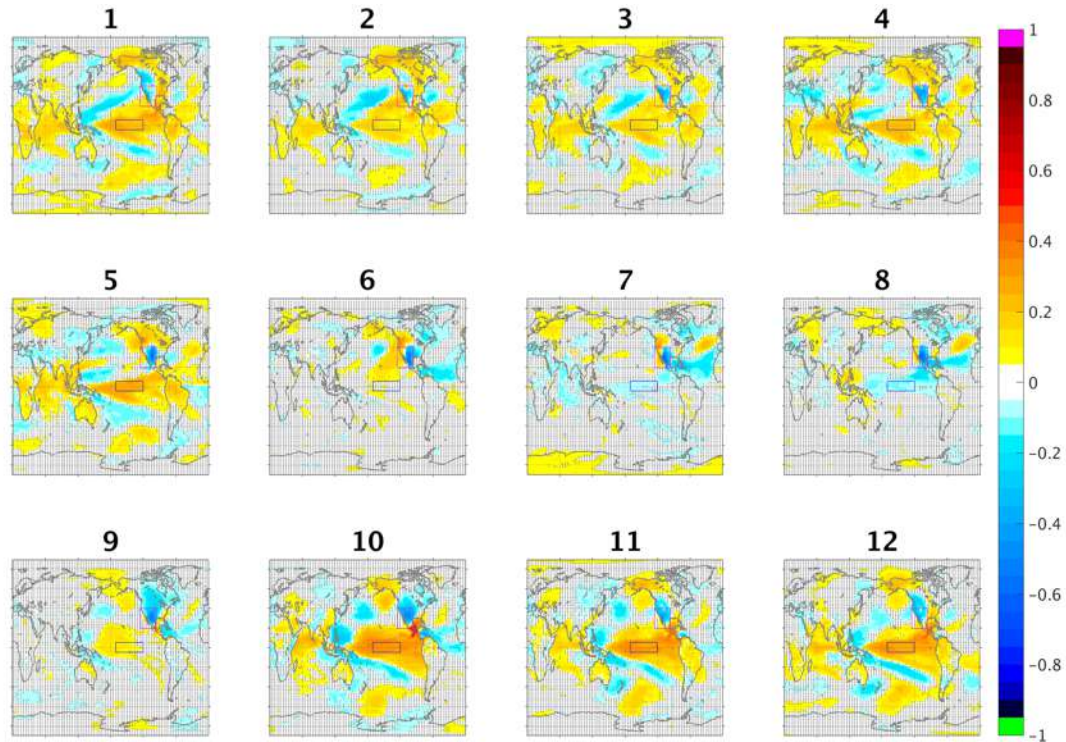


**Fig. 19** Correlation of monthly surface temperature with monthly precipitation averaged over southwestern North America (19-40°N, 125-96°W, indicated by a red box in each panel) as a function of calendar months in FLOR. Gray stippling denotes that the correlation is not significant at 5% level (based on a two-sided student t test). Note that this figure has been published in Zhang (2020, Fig. 13).



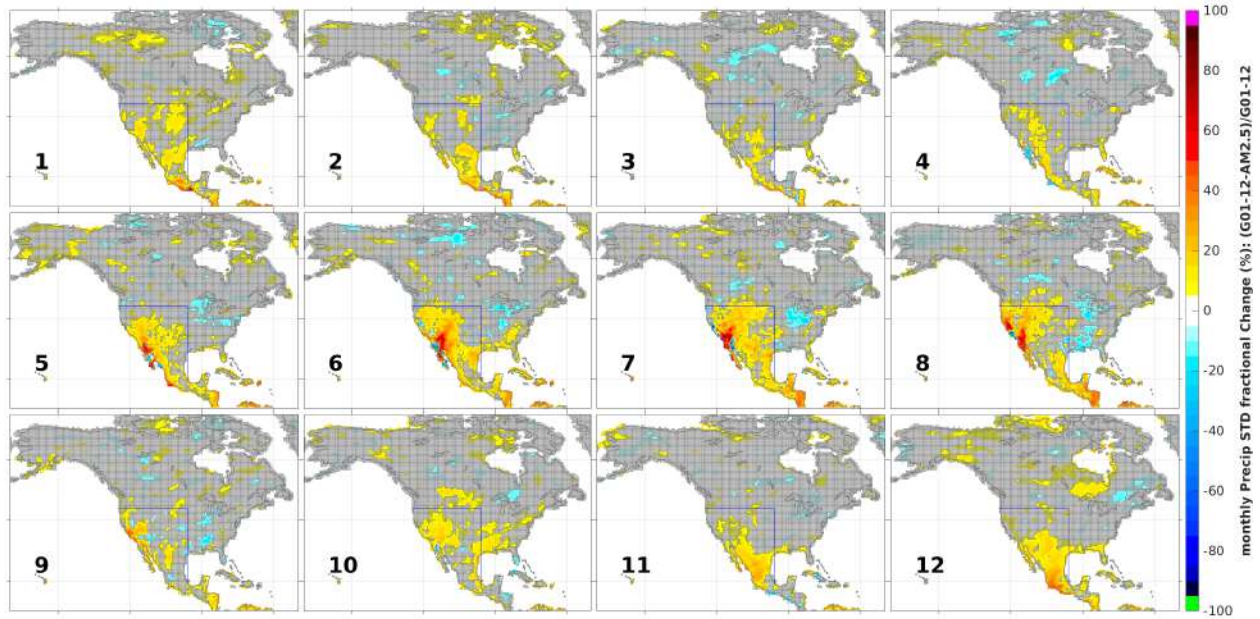


**Fig. 20** Fractional change (%) in year-to-year standard deviation of monthly precipitation in Globe\_1-12 relative to AM2.5,  $(\text{Globe\_1-12} - \text{AM2.5})/\text{Globe\_1-12} \times 100\%$ , as a function of calendar month. Gray stippling indicates changes are not significant at the 1% level based on a two-sided Fisher test.

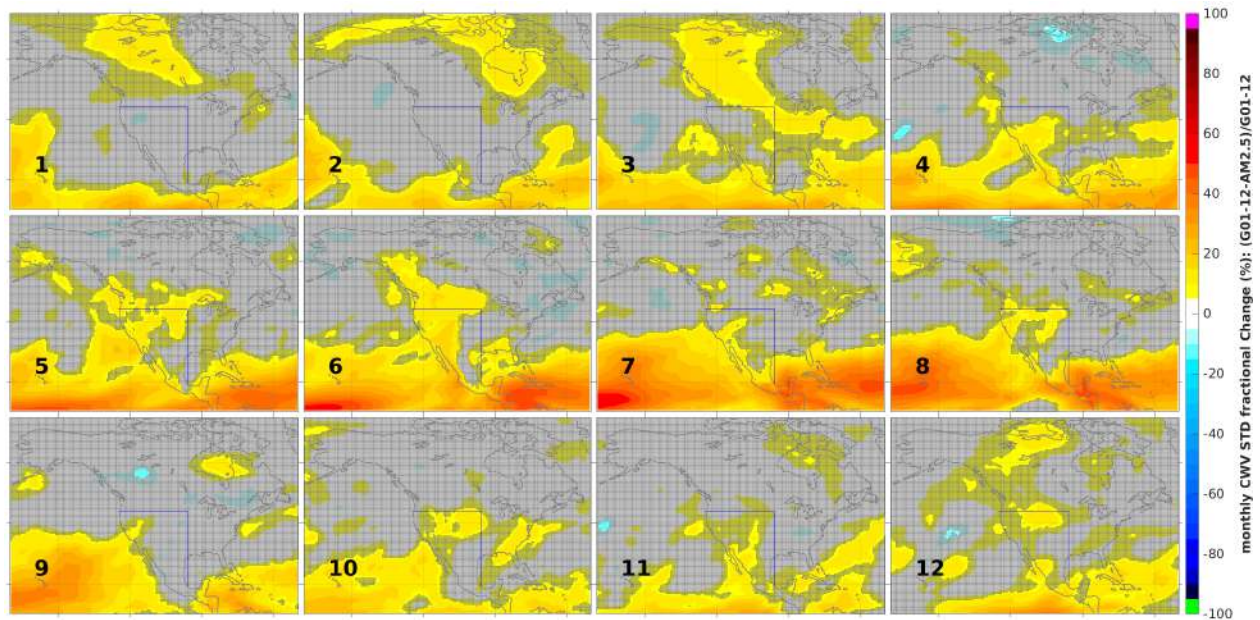


**Fig. 21** The same as Fig. 20 but for CWV in Globe\_1-12.



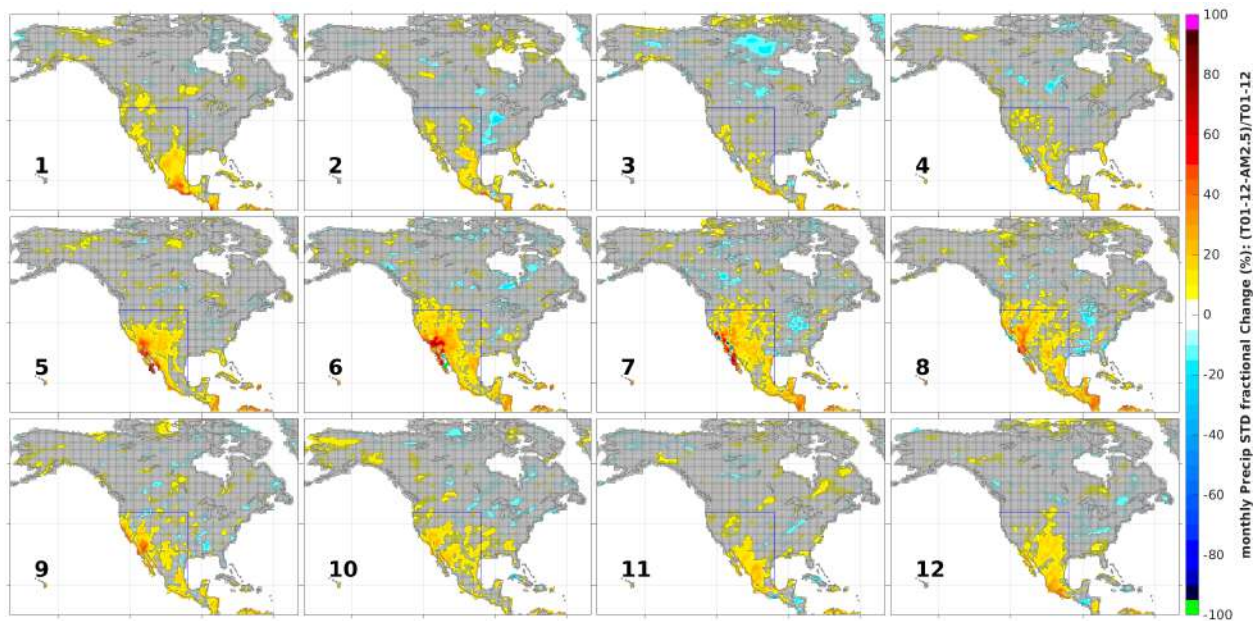


**Fig. 22** The same as Fig. 20 but for Tropic\_1-12.

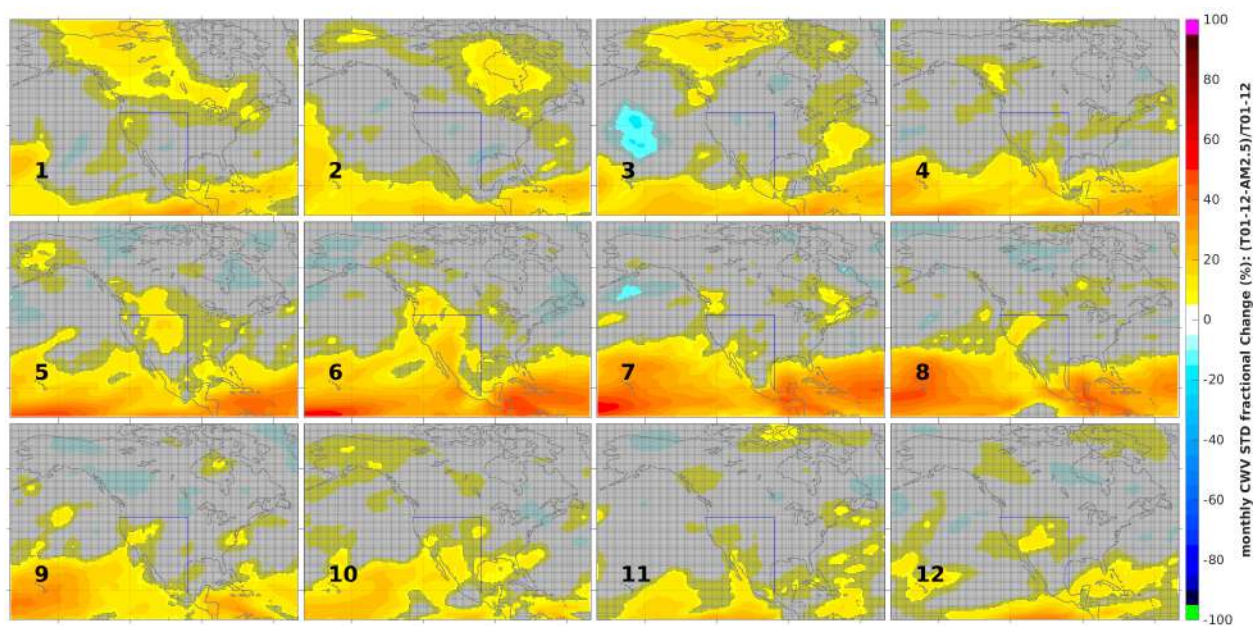


**Fig. 23** The same as Fig. 22 but for CWV in Tropic\_1-12.